PERGAMON

Progress in Aerospace Sciences 38 (2002) 145–180

PROGRESS IN AEROSPACE SCIENCES

www.elsevier.com/locate/paerosci

Prediction of high lift: review of present CFD capability

Christopher L. Rumsey[a,*], Susan X. Ying[b]

[a] *NASA Langley Research Center, Mail Stop 128, Hampton, VA 23681–2199, USA*
[b] *The Boeing Company, Long Beach, CA, USA*

Abstract

A survey is conducted of CFD methods applied to the computation of high-lift multi-element configurations over the last 10–15 years. Both 2-D and 3-D configurations are covered. The review is organized by configuration, in an effort to glean useful insights with respect to particular successes or failings of CFD methods as a whole. In general, for both 2-D and 3-D flows, if certain guidelines regarding grid, transition, and turbulence model are followed, then surface pressures, skin friction, lift, and drag can be predicted with reasonably good accuracy at angles of attack below stall. Velocity profiles can generally be predicted in 2-D flow fields, with the exception of the slat wake, which tends to be predicted too deep by most CFD codes for a range of different configurations. CFD codes can usually predict trends due to Reynolds number in 2-D, but they are inconsistent in the prediction of trends due to configuration changes. On the whole, 2-D CFD is unreliable for predicting stall (maximum lift and the angle of attack at which it occurs); in most cases, maximum lift is overpredicted, but for some configurations the opposite occurs. However, there is some evidence that stall misprediction of nominally 2-D experiments may be caused by 3-D effects, which are obviously not modeled by 2-D CFD. In general, 3-D computations are also inconsistent with respect to computing stall, but there have been fewer of these applications to date. The paper concludes with a list of challenges that confront CFD at the start of the next decade, which should witness a dramatic increase in the number of CFD applications for 3-D high-lift configurations. Published by Elsevier Science Ltd.

Contents

*Corresponding author. Fax: +1-757-864-8816.
E-mail address: c.l.rumsey@larc.nasa.gov (C.L. Rumsey).

0376-0421/02/$ - see front matter Published by Elsevier Science Ltd.
PII: S0376-0421(02)00003-9

Nomenclature

c	chord
C_D	drag coefficient
C_L	lift coefficient
$C_{L,max}$	maximum lift coefficient
C_p	coefficient of pressure
C_{mu}	engine thrust coefficient
k	turbulent kinetic energy
Re	Reynolds number
S_{ij}	kinematic strain rate tensor, $(\partial u_i/\partial x_j + \partial u_j/\partial x_i)/2$
u_i	velocity component
x_i	Cartesian coordinate
Greek symbols	
α	angle of attack
ε	dissipation rate of k
σ	parameter related to suction rate through porous wall
τ_{ij}	turbulent stress tensor
ν_t	kinematic eddy viscosiy
ω	ε/k
Abbreviations	
BB	Baldwin–Barth turbulence model
BL	Baldwin–Lomax turbulence model
CBL	confluent boundary layer
CFD	computational fluid dynamics
DNS	direct numerical simulation
EASM	explicit algebraic stress model
EASMCC	EASM with curvature correction
EET	energy efficient transport
GARTEUR	Group for Aeronautical Research and Technology in Europe
HWT	high-wing transport
IBL	interactive or integral boundary layer
LES	large eddy simulation
LTPT	low turbulence pressure tunnel
MDA	McDonnell Douglas Aerospace
NASA	National Aeronautics and Space Administration
NLR	National Aerospace Laboratory (Netherlands)
ONERA	French National Aerospace Research Establishment
PDR	pressure difference rule
RANS	Reynolds-averaged Navier–Stokes
RSM	Reynolds stress model
SA or S–A	Spalart–Allmaras turbulence model
SARC	SA model with rotation/curvature correction
SST	Menter's $k-\omega$ shear stress transport turbulence model

1. Introduction

1.1. Overview

Engineers are increasingly reliant on computational fluid dynamics (CFD) for the design and analysis of aerospace vehicles. Confidence in industry has been gradually building in the ability of the Reynolds-averaged Navier–Stokes (RANS) equations, as well as simpler coupled Integral Boundary Layer (IBL) methods, to adequately predict the design trends and flow fields of aerospace vehicles with attached flow. Much of this confidence comes as a result of increased computer power, and the consequent ability to more faithfully model the geometries used in the experiments or flight tests.

But no such confidence yet exists for high-lift flow fields, especially those for which significant regions of separated flow are present. Predicting the onset and progression of separated flow with angle of attack, including the effects of Reynolds number (Re), remains an elusive goal. Multi-element airfoils and wings are generally associated with separated flow, along with a host of other flow physics that can be difficult to model accurately (see Fig. 1). In addition, experimental uncertainties also tend to increase for separated flows and for flows at high angles of attack near stall. As a result, it is currently not possible to use CFD to reliably predict $C_{L,max}$ or the angle of attack at which it occurs in experiment. These global properties are important in vehicle design studies.

Considering the CFD process, there are many possible reasons for inconsistent predictions of high-lift flow fields. One explanation is that the models used in the RANS equations cannot describe the turbulent flow physics of some types of high-lift flows. Certainly, if a flow field is unsteady, then at the very least the RANS equations must be solved time-accurately: the time scale of any gross unsteady motion should be much greater than the physical time step employed, which in turn should be much greater than the time scales associated with the turbulence. The turbulence model itself is also problematic. Not only are there many turbulence models to choose from, but there is also little agreement as to which models are applicable in any given circumstance. Other methods with a potentially broader range of applicability, such as large-eddy simulation (LES) and blended RANS–LES capabilities, are emerging today. These methods may some day supplant RANS in the aerospace industry. Note that there is also turbulence

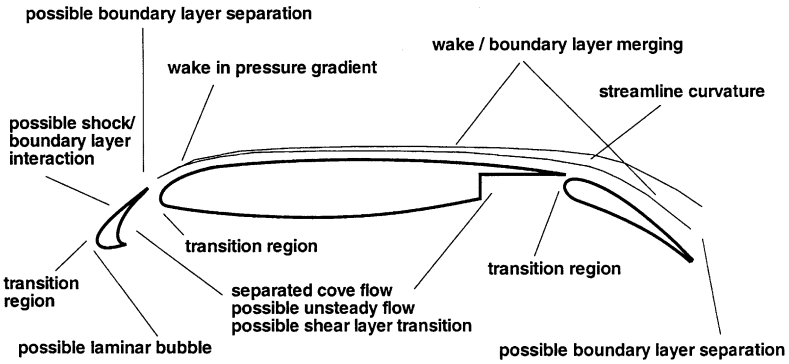

Fig. 1. Challenges inherent in multi-element flow field prediction.

modeling associated with LES methods, although the modeling occurs only for the smallest-scale eddies in this case. Direct numerical simulations (DNS) over realistic configurations at flight *Re* are still well beyond the reach of today's computers.

Finally, both numerical errors and lack of geometric fidelity may result in inadequate or inconsistent CFD results. It is difficult to ensure adequate grid resolution for 3-D complex geometries, and it is easy to overlook or ignore potential geometric inconsistencies and aeroelastic effects. Also, it is rarely cost-effective to fully resolve all aspects of a flow field in a computation. For example, side-wall boundary layers and slotted wall effects in wind tunnels are usually modeled approximately in some way, and undoubtedly introduce some errors. These errors may manifest themselves for *any* flow field, but become particularly important when the dynamics of the flow are very sensitive to small changes in flow field properties or geometry.

1.2. Focus of this work

The focus of the current paper is to provide an overview of present CFD capability applied to the prediction of high-lift flow fields. To accomplish this objective, a review is conducted of research results published within the last 10–15 years, pertaining to the application of CFD to high-lift applications. By summarizing these efforts, a clear picture emerges as to where we stand at the present time, and where additional resources should be focused in the future.

To further limit the scope to a manageable size, consideration is restricted to multi-element configurations, both for 2-D airfoils as well as for 3-D wings and more complex configurations. Application of CFD to single-element airfoils and wings or bodies operating at high lift, such as delta wing or blended-wing/body flows, are not covered here. Because the subject of the paper is CFD capability for computing high-lift flows, we do not discuss in detail experimental programs of research, except as they relate directly to the computations or the physical processes described. For more discussion on experimental issues, see, for example, Hobbs et al. [64], Nield [114], Payne et al. [122], Thibert [161], Woodward and Lean [183], and Yip et al. [186].

The paper is organized as follows. First, a review of high-lift flow physics is given. This section highlights the types of flow features that play a significant role in multi-element flow fields, and which CFD must address with sufficient accuracy. Second, a summary of some of the main computational methods that have been used in the last decade to attack multi-element flows is provided. This section also includes a brief review of some of the more widely-used turbulence models applied to this type of flow. The next section of the paper consists of a detailed review of CFD research conducted over the last 10–15 years for applications to both 2-D and 3-D configurations. Then, lessons learned and conclusions are presented along with challenges for future CFD efforts.

2. Review of high-lift flow physics

For a detailed review of high-lift aerodynamics, the reader is referred to the seminal work of Smith [145]. A discussion on the subject is also included in Brune and McMasters [26], Garner et al. [57], Smith [146], and Ying et al. [185]. Only a few basic general concepts are covered in this section.

Some of the physics pertinent to high-lift flows are sketched in Fig. 1 (shown for a 3-element airfoil section). Separated (possibly unsteady) flow exists in the cove regions of the slat and main elements, and there is possible transition along the shear layers emanating from the cusps. Each element initiates a fresh boundary layer with its own transition region. The flow over the top of the airfoil section can have significant curvature,

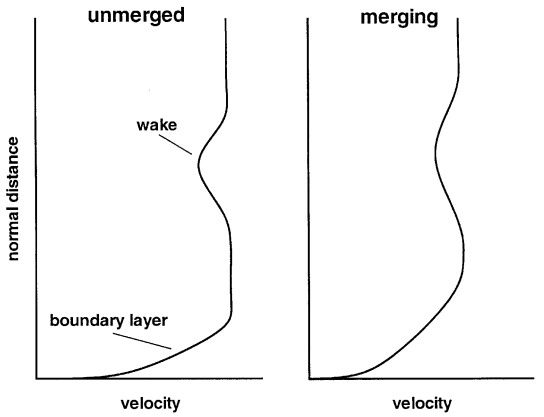

Fig. 2. Typical multi-element velocity profiles, showing wake and boundary layer features prior to and during merging.

and shock/boundary layer interaction and boundary layer separation (on or off the body) is also possible.

The flow field is also characterized by interaction and subsequent merging of each upstream element's wake with the boundary layers of the downstream elements. The wakes themselves are subject to strong variable pressure gradients, often with extended adverse pressure gradient runs. The confluent boundary layer (CBL) over each downstream element consists of the element's boundary layer interacting with wakes from upstream elements, as illustrated in Fig. 2. If the boundary layer and wakes have a large enough separation between them, then there is also a layer or layers of unretarded air from the upstream gaps, which usually disappear further downstream as the layers merge. The CBL can be very thick and extend from the surface well into the flow field (e.g., 20% chord). The CBL can generally withstand a larger adverse pressure gradient (avoiding separation) than a standard boundary layer.

Each of the above-mentioned items alone can be a challenge for CFD methods; together, they represent a formidable task. 3-D flows offer the additional challenges of modeling support tracks, fairings, edge and junction flows, and nacelle/propulsion interaction effects. In these cases, CFD must be able to accurately capture 3-D flow features such as vortices.

Some other aspects of high-lift flow physics, taken from Smith [145], are summarized here. When considering wing design, to get more lift, higher velocities are needed over the wing's upper surface. But higher velocities mean greater decelerations toward the rear, and hence a greater likelihood of separation. According to Smith, there are five primary effects of (properly designed) gaps on multi-element wings that give advantages over single-element wings in this regard. The first is the slat effect: the velocities due to circulation on upstream elements reduce pressure peaks on downstream elements, and boundary layers are better able to negotiate the resulting lowered adverse gradient. The second is the circulation effect: downstream elements causes a flow inclination (effectively a higher angle of attack at the trailing edge of the upstream elements) that induces greater circulation, and hence greater lift, on the upstream elements. The third is the dumping effect: because the trailing edge of an upstream element is in a region of velocity higher than freestream, there is a higher discharge velocity of the boundary layer into the wake than there would be if there were no downstream elements present. This higher velocity reduces the pressure rise impressed on the boundary layer and reduces the likelihood of separation. The fourth is the off-surface pressure recovery: the wakes of upstream elements, formed from boundary layers dumped at higher-than-freestream velocity, decelerate out of contact with a wall. This process is more efficient than deceleration in contact with a wall. The fifth is the fresh boundary layer effect: each new element has its own fresh boundary layer, and thin boundary layers can withstand greater adverse pressure gradients than thick ones.

The mechanisms responsible for limiting the maximum lift attainable on multi-element wing configurations are not well understood. For a typical three-element airfoil at low angle of attack, the main element carries the highest load, followed by the flap and the slat. The lift on the main and slat elements increases with increased incidence, whereas the lift on the flap generally decreases as its pressure suction peak becomes more moderate. This lift curve behavior is illustrated in Fig. 3. At stall, the main element reaches its maximum lift, although not necessarily due to any region of separated flow. In fact, many multi-element airfoils exhibit no separated flow regions at maximum lift, and their lift curves near stall are relatively flat (indicating a gradual

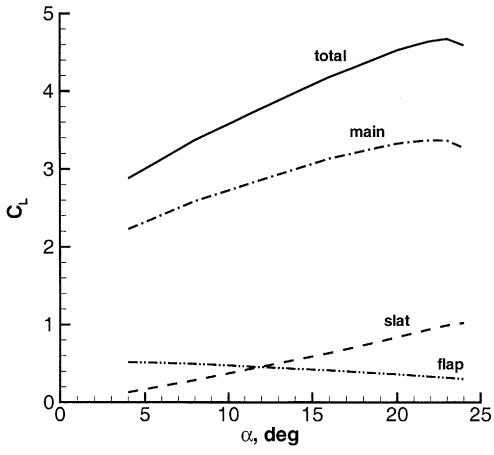

Fig. 3. Typical lift curves for a 3-element airfoil.

stall), unlike the rapid drop off of a leading edge stall often associated with single-element airfoils. Petrov [123,124] noted an off-surface flow reversal region in the wake of the flap surface of a multi-element airfoil that was presumed to limit its maximum attainable lift. Also, Drela [49] found maximum lift to be limited in a computation by the bursting of the main element wake in the pressure gradient of the flap. However, in different experiments [109,164,147], others have reported no evidence of this type of off-surface behavior at maximum lift conditions.

One of the most important needs in the aerospace industry is to be able to use CFD to predict a priori scale effects and configuration effects in wing design. Currently, most wind tunnels operate at lower-than-flight *Re*, and scale effects are poorly understood. Therefore, use of wind tunnel data alone to design a wing can introduce a significant amount of uncertainty. Unfortunately, CFD has not proven itself reliable enough for use in this regard. Currently, it is generally considered reliable only for flight regimes near cruise conditions, when there is little or no separated flow present and when high-lift devices are not deployed.

Haines [62,63] discussed in great detail the issue of scale effects. Five principal scale effects as applied to multi-element airfoils are: (1) decrease of the boundary layer thickness with *Re*; (2) decrease in laminar bubble size with *Re*; (3) a sudden change from bubble-dominated to conventional scale effect on a slat and, possibly, main wing; (4) movement of transition with *Re*; and (5) slot-flow dominated scale effect with *Re* related to flow separations and/or changes in the viscous interaction between the wake of an upstream surface and the flow over a downstream surface. Generally, the first three effects are favorable with increasing *Re*, but the last two effects can be unfavorable. Effect (5) is the most difficult to predict, and depends on how the flow behaves (attached or separated) on the rear surface. Woodward et al. [182] found that after optimizing a gap at low *Re*, by raising *Re* the effective gap increased due to the thinning of the boundary layer. This effective gap increase led to an increase of the peak suction on the aft element, which in turn induced separation near the trailing edge of that element. This type of adverse scale effect can override the favorable effects of increasing *Re* on separation characteristics.

3. Computational methods

In this section most of the computational methods that have been used to compute high-lift flows since the late 1980s are classified and categorized. Broadly speaking, the methods are broken into the two general categories of IBL methods and RANS methods. Within each of these general categories, several specific variations exist, but we do not draw too much of a distinction here. For more details, the interested reader is referred to the cited references. (Note that the Euler equations, which are the Navier–Stokes equations without viscous terms, do not fit into either of these two categories. However, they are only rarely used for multi-element airfoil and wing computations, because viscous effects in these problems are so important. Therefore we do not discuss them here.)

Table 1 lists codes that fall into the general category of coupled IBL-type codes, whereas Table 2 lists RANS codes. Some of the codes were not referred to by name in the original references; these are listed by the reference author. (The eight codes used in Arlinger and Larsson [7] were not named in the reference, so these have been left out of the table.) From these tables, we note that most of the methods applied to multi-element high-lift applications have been RANS codes. The incompressible unstructured-grid RANS code INS2D/INS3D has been used in the largest number of references.

With regard to the RANS formulation, turbulence modeling represents an approximation that can be difficult to quantify. When applications involve complex configurations, it is often difficult to determine whether lack of agreement with experiment is due to the turbulence model or some other issue. It is therefore often very helpful to break complex problems into a series of simplified problems, or "unit problems", and conduct the evaluation of the turbulence models for the simplified problems to uncover specific failings (see, e.g., [16]).

Prior to 1990, most RANS codes utilized simple algebraic (zero-equation) turbulence models such as the Baldwin–Lomax (BL) model [15]. However,

Table 1
Summary of coupled IBL-type codes

Code	CFD ref.
APANEL	[53,121]
Cebeci et al. method	[20–22, 35–37, 173]
FELMA	[8]
HILDA	[8]
ISES/MSES	[48,49,82,187]
Jacob et al. method	[50,68]
Kusunose et al. method	[86]
MCARF	[82,187]
MEAFOIL	[82]
MULTIVIS	[97]
PMARC	[186]
TRANAIR	[53]
Valarezo et al. method	[166]
VILMA	[8–10]
VIS18/VIS18b	[8,89,92,162]
VISWAKE	[8]
VSAERO	[9]

Table 2
Summary of RANS codes

Code	Type	Grid	CFD ref.
AIRUNS2D	Compressible	Unstructured	[92]
ARC2D	Compressible	Structured	[65]
Bartsch et al. method	Compressible	Structured	[17]
CANARI	Compressible	Structured	[92]
CEVCATS	Compressible	Structured	[11]
CFL3D	Compressible	Structured	[18,42,43,53,70,73,76,82,138,139,140,159,185]
CRTVD	Compressible	Structured	[65]
Egami et al. method	Compressible	Structured	[51,143]
EURANUS	Compressible	Structured	[92,95]
FANS	Compressible	Unstructured	[92]
FIDAP	Incompressible	Structured	[83]
FLO103-MB	Compressible	Structured	[79]
FLOWer	Compressible	Unstructured	[9,92,137,179]
Fritz method	Compressible	Structured	[56]
FUN2D/FUN3D	Compressible	Unstructured	[3,4,82,140]
Hyams et al. method	Incompressible	Unstructured	[67]
INS2D/INS3D	Incompressible	Structured	[12,31,32,46,47,52,53,61,74,75,82,84,85,91,93,94,99,121,130,132,136]
ISAAC	Compressible	Structured	[66,108]
Johnston et al. method	Compressible	Unstructured	[29,30,69,72,151,152,153,160]
Kim et al. method	Incompressible	Structured	[77]
Kim et al. method	Compressible	Structured	[77,78]
Larsson method	Compressible	Structured	[88]
MELINA	Compressible	Structured	[9]
NASTD	Compressible	Structured	[74]
NS2D	Compressible	Structured	[92]
NSMB	Compressible	Structured	[41]
NSU2D/NSU3D	Compressible	Unstructured	[23,53,82,98,100,101,107,126,169,186]
OVERFLOW	Compressible	Structured	[12,33,53,110,131,133–135,144]
PARC2D	Compressible	Structured	[39,40]
PASSABLE	Incompressible	Structured	[2]
RANSMB	Compressible	Structured	[53,92]
Ravachol method	Incompressible	Unstructured	[129]
Schuster et al. method	Compressible	Structured	[142]
STREAM	Compressible	Structured	[90]
TAU	Compressible	Unstructured	[137]
TLNS3D	Compressible	Structured	[82,158]
TORNADO (ARC2D)	Compressible	Structured	[45,53,59,111–113]
Wilquem et al. method	Incompressible	Structured	[181]
ZEN	Compressible	Structured	[92]

two-equation turbulence models such as the $k-\varepsilon$ and the $k-\omega$ models (see [178]) had also started to make their way into RANS codes. Unfortunately, there were (and still are) a lot of variations on these models, and it can be difficult to keep track of them, much less understand their relative merits with respect to high-lift CFD. Throughout the remainder of this paper, we generally group $k-\varepsilon$ and $k-\omega$ models into two broad categories for simplicity, except where additional differentiation is warranted. In general, the BL model and most of the $k-\varepsilon$ and early $k-\omega$ models performed poorly for wall-bounded separated flows caused by adverse pressure gradients.

During the first half of the 1990s, three turbulence models were developed that had a significant impact on RANS codes in the aerospace industry. Specifically, they improved the ability to predict separated flows while maintaining good results for attached flows as well. Because of their importance and wide use, we cite them here. Baldwin and Barth [14] developed a one-equation model (BB), which was used extensively at the time and also inspired later models. However, this model is

generally no longer considered viable because the formulation is ill-conditioned near the edge of boundary layers [104]. The Spalart–Allmaras (SA) one-equation model [148] is one of the most widely-used turbulence models today. It is known to give poor predictions in jet flows and it has a tendency to overdiffuse free vorticity, but it is extremely robust and does well for 2-D mixing layers, wake flows, and boundary layer flows. Finally, Menter [103] developed a model that represented a blend of the $k-\omega$ and $k-\varepsilon$ models, and included a shear stress transport term that improved the model's performance for adverse pressure gradient wall-bounded flows. This model is written in the $k-\omega$ form, and is referred to as the SST model.

Most turbulence models in use today (including those described above) are linear models, which assume that the turbulent shear stress is directly proportional to the strain, so that $\tau_{ij} = -2\nu_t S_{ij}$ (also referred to as the Boussinesq assumption). It is not yet clear precisely how valid or invalid this assumption is for multi-element high-lift flows, although some research into this issue has been started [138,185]. Other models that are higher in the hierarchy of complexity and physical realizability do not make this linear assumption. For example, explicit algebraic stress models (EASM) include non-linear terms in the relation for turbulent shear stress, and still can be implemented in a two-equation framework [138]. Full Reynolds stress models (RSM) represent the most complete approximation level in a RANS framework, and require the solution of additional turbulence equations. To date, very few production-type codes for complex configurations possess RSM capability.

4. Review of research

In presenting a review of the computational research on multi-element configurations over the last 10–15 years, we have chosen to break the summary down by configuration. General successes or failures are assessed as a function of configuration, and patterns regarding suitability of particular methods or turbulence models for particular physical characteristics emerge.

Previous reviews of CFD research for high-lift flows, or reviews of numerical issues associated with computing such flows, can be found in Balasubramanian et al. [13], Brune and McMasters [26], Garner et al. [57], King and Williams [80], Lynch et al. [98], Meredith [105], Squire [149], Valarezo [165], and Ying [184]. Although not covered in detail in this paper, grid generation itself can be difficult and important for multi-element configurations. See, for example, Cao and Kusunose [31], Moitra [107], Rogers et al. [131], and Rogers et al. [135].

The field of design optimization has seen an explosive growth in recent years. Because one of the challenges in multi-element airfoil and wing design is the relative placement of the elements, multi-element design can clearly benefit from automated optimization techniques. Although this subject is not directly covered in this paper, many multi-element optimization studies have been conducted. See, for example, Alexandrov et al. [3], Besnard et al. [22], Drela [49], Eyi et al. [52], Greenman and Roth [61], Kim et al. [78,79], and Wild [179].

Tables 3–5 give a summary of all multi-element configurations computed using CFD. They are organized as follows: Table 3 lists 2-D configurations for which experimental citations exist ("exp ref"), Table 4 lists 3-D configurations for which experimental citations exist, and Table 5 lists both 2-D and 3-D configurations for which *no* experimental citations exist. The references corresponding to the computations are given under the heading "CFD ref". These tables list every multi-element configuration found during an extensive literature survey. However, it is certainly possible that some relevant computational references have been inadvertently overlooked. On the other hand, the experimental references are not intended to be exhaustive; i.e., only those believed to be directly relevant to the particular configuration(s) computed are listed here. In the case of Table 5, no experimental references are given at all because they were not listed in the references (presumably because the data was either preliminary or proprietary).

In Table 3, Rumsey et al. [140] is unique in that it used 3-D computations to compute the nominally 2-D McDonnell Douglas Aerospace (MDA) 3-element airfoil flow field. However, this reference was grouped with the other 2-D cases because the experiment was designed to produce a 2-D dataset. More will be said about this reference later.

We make the following general observations regarding Tables 3–5. First, the interest in multi-element computations has been considerable over the last decade, and many CFD papers have been written about them. Most papers (on the order of 100) deal with 2-D computations of nominally 2-D flows. About one-fourth as many references deal with 3-D multi-element computations, but recent years have seen an increase in the rate of publications in this area. Second, most of the cases are at low speed ($M < 0.3$) and at low Reynolds numbers typically achieved in most wind tunnels ($Re < 10$ million). The highest Reynolds number cited is $Re = 23$ million. Finally, although many of the cases were computed in only one or two references, several have been computed in larger groups of references. When a large group independently computes a particular case, we can get a better sense of the CFD capabilities and

Table 3
Summary of 2-D multi-element configurations

Configuration	Element	Exp ref.	$Re \times 10^6$	M	CFD ref.
CCM	2	[2]	0.3	?	[2]
Fighter-type	2	[46,64]	5–16	0.2	[46,75]
Foster	2	[55]	3.8	?	[83]
GA(W)-1 + fowler	2	[174,175]	2.2	0.13–0.21	[83,97]
GA(W)-1 2-element	2	[24,25]	0.62	0.15	[59,70,112,113,142]
NLR-7301	2	[60,170,171]	2.51	0.2	[7,10,29–31,35,36,56,59,69,70,72,74,77,80,83,84,86,88,90, 112,129,151,152,160]
Omar 2-element	2	[117,118]	2.83	0.201	[35,36,97]
Payne	2	[121]	2.5–23.0	0.18	[107,121]
SKF 1.1	2	[150]	2.2	0.6–0.76	[69,72,112,151,153]
Whitcomb-Clark	2	[177]	9	0.75	[3]
Williams	2	[180]	1.2	?	[181]
4412 + 4415 (A)	2	[1]	1.8	0.09	[17,136,113]
4412 + 4415 (B)	2	[116]	1.3	0.06	[173]
Fiddes	3	[54]	10	0.18	[80]
GA(W)-1 3-element	3	[24,25]	0.62	0.15	[70,77,113]
GARTEUR A310	3	[8,161]	1.9–16	0.13–0.3	[9,10,88,92,95,162]
GARTEUR M3	3	[172]	1.9	0.22	[56]
Laia	3	[87]	3.4	0.17	[40]
MDA 3-element (30P-30N, others)	3	[19,38,81,102,140, 147,167,168]	5–16	0.2	[4,21–23,32,42,43,47,52,73,74,79,82,93,94,98,107,108,126, 130,132,136,138–140,169,185]
NASA 3-element	3	[91]	4.2–16	0.2	[91]
NHLP-2-D	3	[28,106]	3.52	0.2	[36,37,45,53,66,108,111,139,156,179]
Omer	3	[119]	2.3–15	?	[85]
RA16SC1	3	[125]	1.8	0.123	[89,162]
Szodruch	3	[157]	1.6	?	[17]
Brune-Sikavi	4	[27]	2	0.16	[48]
MDA 4-element	4	[167,168]	9	0.2	[23]
Omar 4-element	4	[117,118]	2.83	0.201	[49,70,86,97,107,136]

state-of-the-art because code-dependent issues can be filtered to some extent. The cases that were computed in 5 or more references are: GA(W)-1 2-element, NLR-7301, GARTEUR A310, MDA 3-element, NHLP-2D, and Omar 4-element. We first focus on details concerning these particular 2-D cases, then summarize general observations from all 2-D cases. Finally, we give a summary of key findings from 3-D cases. Several representative figures taken from a few selected references appear in the following sections. The figures were chosen primarily in an effort to highlight certain capabilities and limitations of CFD for high-lift flows, but we were far from being all-inclusive in our selection.

Note that in the list of references, there are two bound proceedings that focus exclusively on high-lift issues: AGARD CP-515 (1993) [11,17,35,40,44,56,68,70,72,89, 105,136,161,183,187], and high lift and separation control, proceedings of the conference, RAE (1995) [8,9,63,90,114,124,156,162,186].

4.1. GA(W)-1 2-element

The GA(W)-1 2-element cases are two of five multi-element configurations tested at the Lockheed-Georgia Experimental Research Facility in the early 1980s. Local blowing at the wall was used to improve the 2-D tunnel flow quality. The two cases discussed here consist of a main element and a flap at $Re = 0.62$ million: Case B has the flap set at 30°, and Case C has the flap set at 40°. These are typical of landing flap configurations. Even at low angles of attack (e.g., $\alpha = 4°$), there is a large region of separated flow on the upper surface of the flap in these cases, which represents a challenge for CFD methods.

Schuster and Birkelbaw [142], among the first to compute multi-element airfoil flow using a structured-grid RANS code, computed Case B. Because this work was done so long ago, it is unreasonable to expect too much from the computations: the grid was very coarse (only 117×21, or 2457 total points), and the algebraic

Table 4
Summary of 3-D multi-element configurations

Configuration	Element	Exp ref.	$Re \times 10^6$	M	CFD ref.
DLR-ALVAST	3	[127]	2	0.22	[137,141]
EET	3	[115]	1.35	0.22	[166]
EET aeroecoustic	2 & 3	[18]	3.6–19.2	0.125–0.3	[18]
EET take-off	4	[58]	1.6	0.2	[101,158]
Full-span flap	2	[6]	3.3	0.15	[73]
LFC	3	[5]	2.36	0.1	[50,68]
Lovell wing	3	[96]	1.35	0.22	[20,21,35,166]
NACA 63_2–215	2 & 3	[128,154]	3.7	0.2	[12,76,159]
Part-span flap	2	[176]	3.3	0.15	[73]
Storms part-span	2	[155]	3.7	0.2	[100]
Trap wing	3	[71]	3.7–15	0.15–0.2	[110,134]
WBL324	5	[187]	2–20	0.18	[126,186]

Table 5
Summary of multi-element configurations for which there is no experimental citation

Configuration	$Re \times 10^6$	M	CFD ref.
2-D Karman–Trefftz	?	0.15	[11]
2-D 3-element	3.4	0.17	[39]
2-D NLR422	?	0.2	[44]
2-D M1	?	0.22	[44]
2-D 3-element	2.32	0.185	[51]
2-D 4-element	1.36–20	0.093–0.185	[51]
2-D 3-element	3.7	?	[61]
2-D NREL S809	1	0.13	[65]
2-D DA4E 4-element	1.4	0.15	[10]
2-D Boeing 4-element	12	0.2	[31]
2-D PR8 2-element	1–1.5	?	[83]
2-D 3-element	3.6	?	[129]
2-D 4-element	?	0.22	[156]
3-D 747PD	8	0.2	[33,131]
3-D HWT	?	0.3	[37]
3-D swept 3-element	1.8	0.18	[68]
3-D EET wing-body	1.6	?	[67]
3-D full-span flap	3.7	?	[99]
3-D part-span flap	3.7	?	[99]
3-D 777-200	5.8	0.2	[133]
3-D Boeing 3-element	2.3	0.184	[143]
3-D HWT	13	0.175	[144]
3-D laminar wing with flap	4.9	0.2	[9]
3-D ALVAST-WB-HL	?	0.18–0.22	[41]

BL turbulence model was employed. With such a coarse grid, computed surface pressures tended to be "ragged". Pressures on the main element upper surface were underpredicted in magnitude, resulting in low values for lift.

More recent computations for Case B (at a low angle of attack of $\alpha = 4^\circ$ only) were done during the 1990s by a group at the University of Toronto and de Havilland Inc. using a structured-grid RANS solver. Over several years, their results steadily improved. Initial computations [112,113] used grids between 60,000 and 100,000 total points and either the BB or SA turbulence model. Later computations [59] used 106,000 total points (mostly increased streamwise density on the upper surface of the flap) and the SA and SST (Menter) models.

In the latter work, both the SA and SST models gave very similar results for this case, with the SST model giving pressures in the separated region on the flap in somewhat better agreement with experiment (Fig. 4). Velocity profiles (Fig. 5), including the main element wake, were predicted similarly by both models in reasonable agreement with experiment (results at STN 56 for Menter in this figure are slightly different from the figure in Godin et al. [59]; the original figure had an error, and has been corrected by the original authors). Turbulent shear stress profiles were also similar between the two models, but did not agree quite as well with the experiment, particularly in the main element's wake region.

Jasper et al. [70] computed Case C (at low angles of attack only). Their structured grid had approximately 25,000 total points, and they used the BL turbulence model. They only showed comparisons with surface pressures, which were in reasonably good agreement with experiment at angles of attack of $\alpha = 4^\circ$ and 8°. There were some discrepancies near the leading and trailing edges.

To summarize results for the GA(W)-1 2-element configuration:

- For this case with separated flow, two modern turbulence models (SA and SST) were similar, and agreed well with experimental surface pressures and velocity profiles.

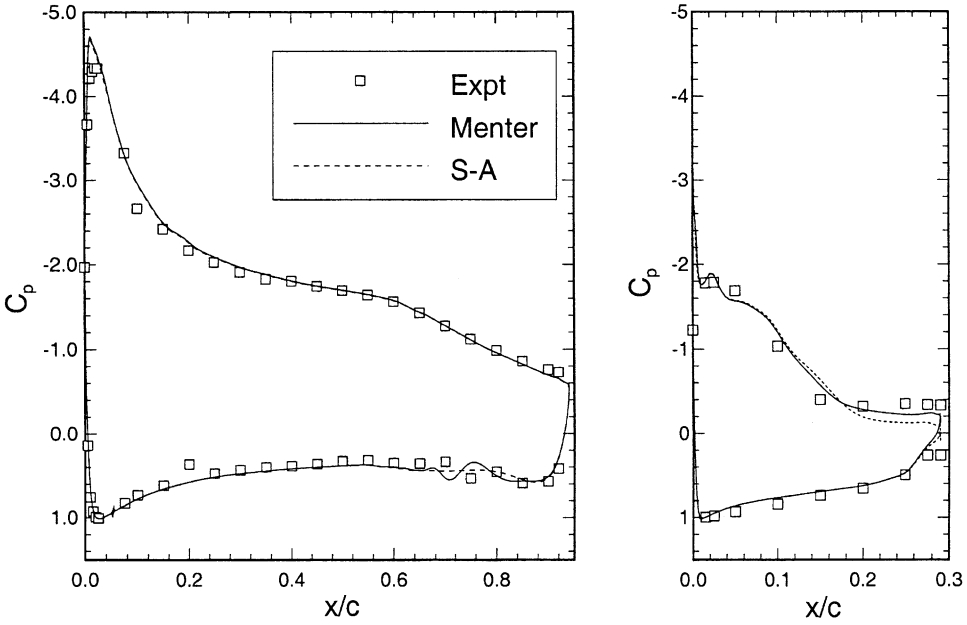

Fig. 4. Pressure distributions for the GA(W)-1 airfoil, from Godin et al. [59]. Copyright © 1997 by the American Institute of Aeronautics and Astronautics, Inc. Reprinted with permission.

- Predictions of turbulent shear stress were also similar between SA and SST, but differed from experiment in some regions of the flow.
- A grid with 106,000 points yielded better comparisons with experiment than coarser grids.

4.2. NLR-7301 2-element

One of the most computed multi-element configurations has been the NLR-7301, a two-element flapped configuration tested in the NLR 3×2 m low-speed wind tunnel in the 1970s. This configuration was designed with moderate flap angle (20°) so that no flow separation would occur on the flap. It is representative of a typical take-off flap setting. Blowing slots were used at the side walls in the tunnel to avoid early flow separations at the model/wall junctions. The presence of a small laminar separation bubble on the wing nose was unavoidable, but because it was small it was felt to have only a very local effect [170]. Two configurations were tested at $Re = 2.51$ million: a gap width of 2.6% c and a gap width of 1.3% c. In both cases, the overlap was the same (5.3% c). In this section, we highlight and summarize some of the results obtained for this configuration. Not all references noted in Table 3 are mentioned.

Arnold and Thiele [10] used a Laplace interaction law in combination with an IBL method to compute the polars, which agreed well everywhere except near maximum lift, where lift was overpredicted. At $\alpha = 13.1°$, the calculated displacement thickness of the wing wake over the flap was underestimated. The ΔC_L trend between the two gap sizes was reasonably well predicted, however.

Cantariti and Johnston [29,30] used an unstructured-grid RANS code for the 2.6%-gap case, and compared two turbulence models: $k-\varepsilon$, and a differential RSM. Both of these models used wall functions. The grid contained approximately 15,000 cells. At $\alpha = 13.1°$, just before the stall angle, both models agreed well with each other and with experiment in lift and surface pressures. Skin friction levels were predicted to be somewhat too high. Past maximum lift, the RSM yielded a more rapid stall, in better agreement with experimental lift levels. However, no experimental surface pressures were available for comparison beyond $\alpha = 13.1°$.

Cao and Kusunose [31] computed the 2.6%-gap case using a structured-grid incompressible RANS code. Their grid had a total of 50,000 points. Surface pressure coefficients generally agreed with experiment, except upper surface levels on the main element were slightly low in magnitude. As a result, lift levels were also low. They attributed the difference to the use of fully turbulent computations, as opposed to specifying transition to match experiment.

Cebeci [35,36] used an IBL approach to compute the 2.6%-gap case. Surface pressure coefficients, lift, and drag levels agreed very well with experiment. Even the angle of attack of maximum lift was predicted

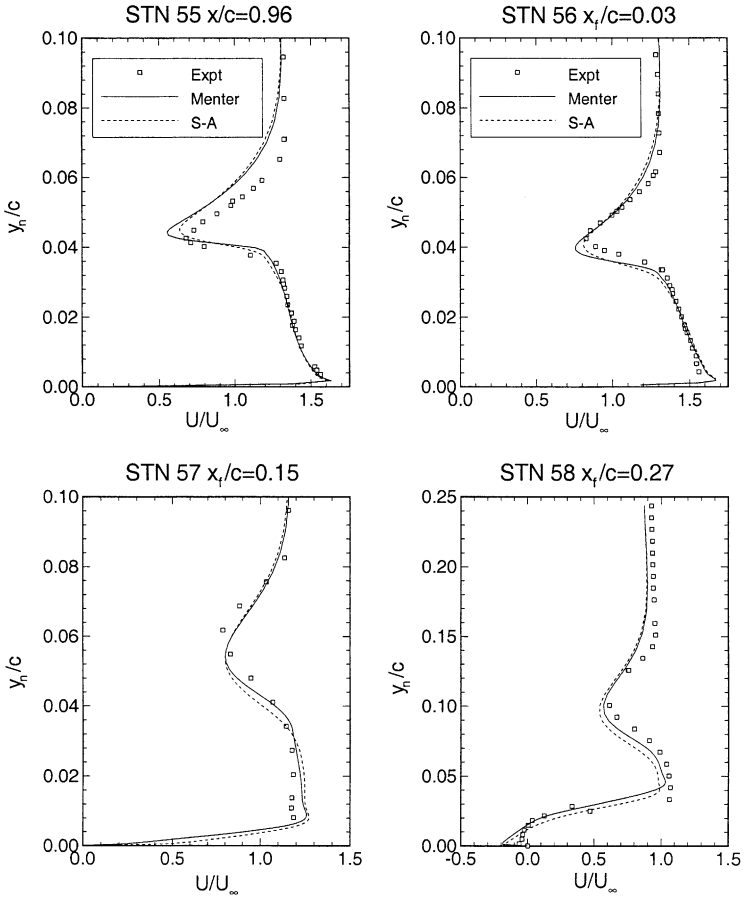

Fig. 5. Velocity profiles for the GA(W)-1 airfoil, from Godin et al. [59]. Copyright © 1997 by the American Institute of Aeronautics and Astronautics, Inc. Reprinted with permission.

in good agreement. Accounting for wake effects (extending the calculations into the wake and modifying the turbulence model in that region) was shown to be important: without it, lift was significantly overpredicted.

Fritz [56] used RANS on a structured-grid with a $k-\varepsilon$ model to compute the 2.6%-gap case. Predicted lift levels were reasonable, but surface pressures on the upper surface of the flap did not agree as well with experiment as other references, particularly at $\alpha = 6^{\circ}$.

Godin et al. [59] used a grid with over 180,000 points to compute both the 2.6%- and 1.3%-gap cases using a structured RANS code. They performed a grid sensitivity study, and were very thorough in attempting to model the experiment as accurately as possible. For example, they noted that in the 2.6%-gap case, a small deflection of the gap was seen in the experiment: they used the measured value of 2.4% c rather than the nominal value, along with an estimated actual flap angle of 19.75°. Transition was fixed to match experiment on both elements, and streamwise grid resolution was increased in the region of the laminar bubble on the main element. The care used in the computations paid off. Surface pressure (Fig. 6) and skin friction coefficients using both SA and SST (Menter) agreed extremely well with experiment. Velocity profiles (Fig. 7) also matched experiment in general, with minor differences exhibited between the two models. Turbulent shear stress profiles showed worse agreement, but the general character was captured overall. The SA model was somewhat better than SST in comparison with experimental turbulent shear stress profiles, and was also better able to capture the effects of the gap variation.

Jahangirian and Johnston [69] computed the 2.6%-gap case at $\alpha = 13.1^{\circ}$ using an unstructured-grid RANS code with grid-adaption capability. Grid adaption had little effect on computed surface pressures (which agreed well with experiment), but it improved skin friction comparisons (although results were too high even after improvement). Their initial grid had only 12,502 cells. Results were obtained with a $k-\varepsilon$ turbulence model and wall functions.

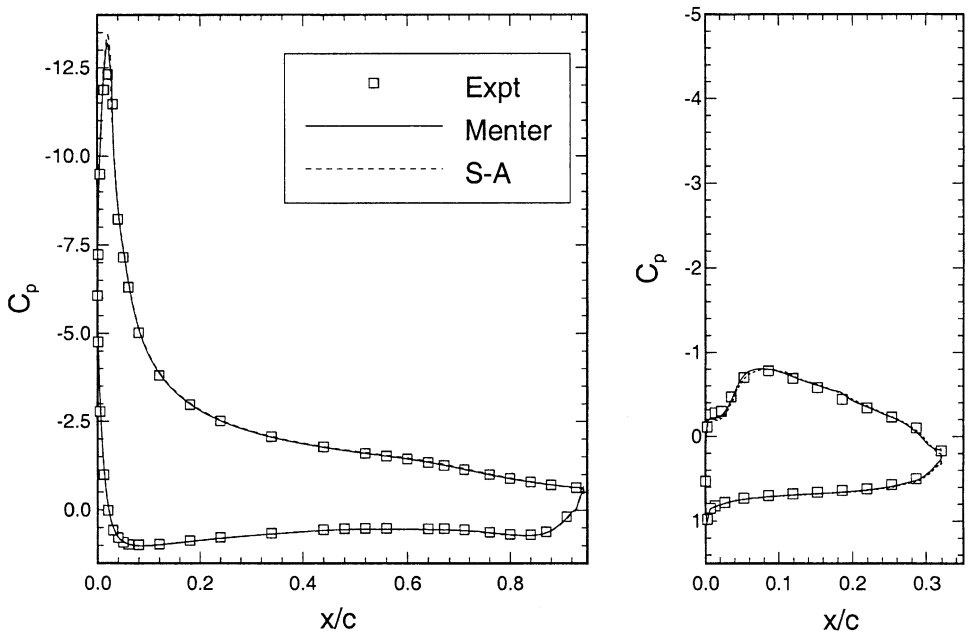

Fig. 6. Pressure distributions for the NLR-7301 airfoil, from Godin et al. [59]. Copyright © 1997 by the American Institute of Aeronautics and Astronautics, Inc. Reprinted with permission.

Jasper et al. [70] computed both NLR-7301 configurations using a structured-grid RANS solver, on a grid with over 46,000 points. They also performed a grid sensitivity study, which indicated that use of a coarser grid (15,000 points) resulted in overprediction of lift levels. They used both the BL and the BB turbulence models. Computed pressures, skin friction, and lift levels agreed well with experiment for both configurations. However, past maximum lift, the computations indicated a higher angle of attack for stall, and a more gradual stall than seen in experiment. The BB model yielded velocity profiles in better agreement with experiment than BL, and somewhat improved behavior near stall. Drag levels were overpredicted by a factor of 2–3.

Johnston and Stolcis [72] used unstructured-grid RANS with a $k-\varepsilon$ turbulence model to compute the 2.6%-gap case. Their grid contained over 12,000 cells. Computed surface pressures agreed well with experiment, and velocity profiles matched experiment for $\alpha = 6^\circ$, but some smearing of results was seen at $\alpha = 13.1^\circ$ due to inadequate grid resolution in the outer wake region. Lift levels were predicted well up to $C_{L,max}$, but stall angle was overpredicted. Drag was significantly overpredicted (by about a factor of 2). Stolcis [151,152] included the use of both an algebraic stress model and a RSM, and showed that these models better predicted separation at and beyond the stall angle, although the rapid loss of lift seen in the experiment was not predicted.

Kim et al. [77] computed the 2.6%-gap case using a structured-grid RANS code on a grid with over 25,000 points. Three different turbulence models, $k-\varepsilon$, $k-\omega$, and SST, gave similar predictions of surface pressures, in good agreement with experiment. Skin friction was predicted well by $k-\omega$ and SST, but was overpredicted by $k-\varepsilon$. Velocity profiles predicted by $k-\omega$ and SST agreed well with each other and with experiment. The $k-\varepsilon$ model yielded poorer results. An incompressible formulation led to worse results than a compressible formulation at $\alpha = 13.1^\circ$ near the suction peak (compressibility effects were significant because the local Mach number was large). The steady-state numerical method used in this reference yielded unsteady massive separation at $\alpha = 13.1^\circ$, but running time-accurately produced converged, attached results.

Kusunose and Cao [84] used an incompressible structured-grid RANS code with built-in transition and the SA turbulence model to predict flow over the 2.6%-gap case. The transition method predicted the transition locations fairly well, and surface pressures and skin friction were in good agreement with experiment, except that the main element suction peak was underpredicted. The grid had 70,000 points.

Kusunose et al. [86] used a viscous/inviscid coupling code with capabilities for predicting laminar, transitioning, or turbulent flows, for the 2.6%-gap case. Surface pressure coefficients and boundary layer properties were predicted in good agreement with experiment,

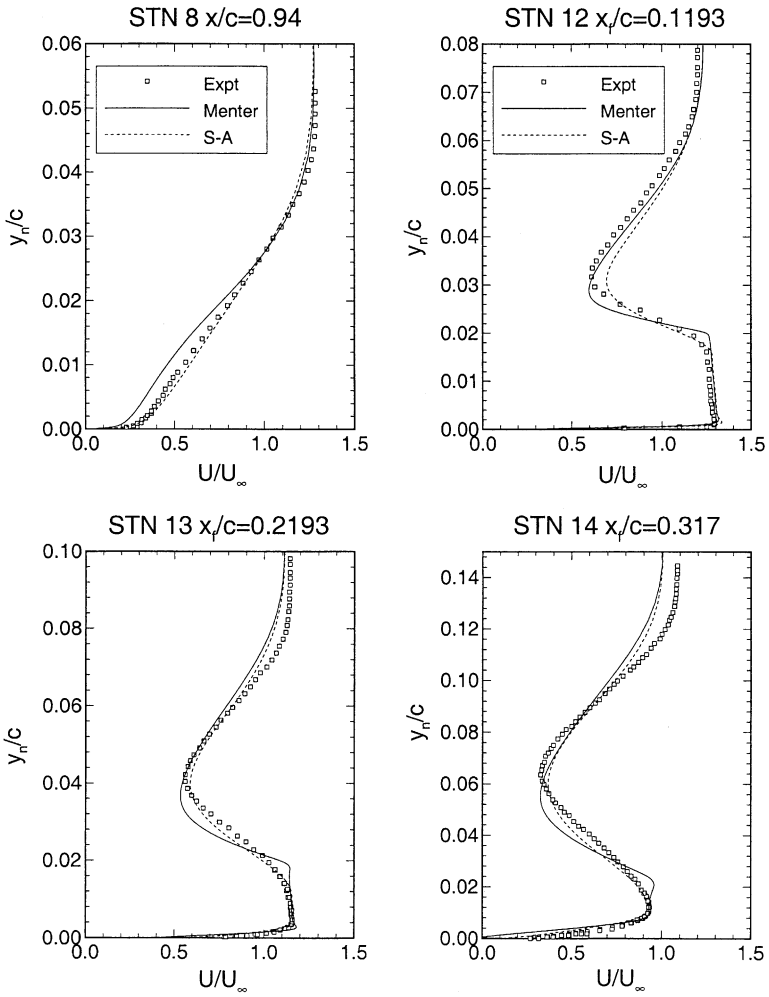

Fig. 7. Velocity profiles for the NLR-7301 airfoil, from Godin et al. [59]. Copyright © 1997 by the American Institute of Aeronautics and Astronautics, Inc. Reprinted with permission.

although lift levels and stall angle were both overpredicted.

Larsson [88] computed the 2.6%-gap case using a $k-\varepsilon$ turbulence models with a structured-grid RANS code. The grid had over 37,000 points. Surface pressure coefficients agreed well with experiment. Skin friction coefficients were predicted slightly high on the main element. Limited velocity profiles showed fairly good agreement, and turbulent shear stress profiles showed fair agreement. To accurately predict drag, it was found necessary to either (a) have the far field grid extent at least to $50c$, or (b) include a far field circulation correction in the boundary condition [163].

Lien et al. [90] used a structured-grid RANS code to compute both the 2.6%-gap case and the 1.3%-gap case. The grids contained over 36,000 points, and a $k-\varepsilon$ model was employed. Surface pressures agreed with experiment, but skin friction levels were somewhat high over the main element. Velocity profiles and turbulent shear stress profiles showed similar agreement as other references.

Nelson et al. [112] computed the 2.6%-gap case using a structured-grid RANS code and the two turbulence models BB and SA. A grid study was conducted: differences between the finest grid with 180,000 points and a grid with 90,000 points was $<1\%$ in lift but nearly 7% in drag. This study indicated that 90,000 points was sufficient for capturing lift (and surface pressures), but not for drag. Although surface pressures agreed well with experiment for both models, lift tended to be slightly overpredicted, and the stall was not computed until $\alpha = 17^{\circ}$, well past the stall angle seen in the experiment. However, the authors noted that the computed laminar bubble was unstable at higher angles of attack, and the abrupt stall seen in the experiment seemed indicative of a leading-edge stall. Hence the stall

break could be computed within a wide range of angles of attack, depending on the choice of transition location in the bubble. By using a measured gap of 2.4% c and flap angle of 19.75° (due to aeroelastic deformation in the tunnel) as opposed to the nominal gap and angle, pressures and forces were not affected significantly, but velocity profiles were improved.

The NLR-7301 configuration was the subject of a CFD validation challenge in Europe, the results of which are summarized in Arlinger and Larsson [7]. The two mandatory cases were: 1.3%-gap at $\alpha = 6^\circ$ and 2.6%-gap at $\alpha = 13.1^\circ$. A standard structured grid with over 36,000 points was used. Overall, as seen in many of the other references cited above, RANS codes did extremely well on these cases. There was more spread in skin friction than in surface pressures, particularly due to sensitivity to how and where transition was turned on. Lift was generally overpredicted, but by $<5\%$. Most codes gave drag levels to within $\pm 10\%$ of the experimental levels. (The importance of the far field circulation correction boundary condition [163] was noted.) Velocity profiles were good overall, even at the highest angle of attack (although there were a few poor results). Turbulent shear stress profiles were worse, but were still qualitatively reasonable. Out of the many turbulence models employed, there was no clear indication that any specific model gave the best results overall. For global quantities, the simple algebraic BL model was as good as any of the more complex models. However, two-equation models generally gave the best predictions of turbulent shear stress profiles.

To summarize results for the NLR-7301 2-element configuration:

- For this attached flow, most CFD methods gave surface pressures that were in very good agreement with experiment.
- Accounting for aeroelastics and transition improved predictions.
- For IBL to do well, modifications to better account for wake effects were necessary.
- The trend between different gap sizes could generally be reasonably predicted.
- $C_{L,max}$ tended to be overpredicted.
- The $k-\varepsilon$ models tended to overpredict skin friction and to give worse agreement with experimental velocity profiles than other models.
- SA and SST models yielded generally similar results.
- The compressible RANS formulation gave better results than incompressible near maximum lift.
- Drag was sensitive to the far field grid extent and/or boundary condition.
- Grids larger than 90,000 points were required for grid independence of drag, but lift and surface pressures were less grid-sensitive.

4.3. GARTEUR A310 3-element

The GARTEUR A310 configuration is a 2-D configuration derived from the 59% station of the Airbus A310 wing. Two high-lift configurations—for take-off and for landing—were tested between $Re = 1.9$ and 16 million via two wind tunnel models in the ONERA F1 and NLR HST and LST tunnels. Wall boundary layer blowing was activated in an attempt to achieve as 2-D a flow field as possible. Maximum lift on this configuration occurs prior to the appearance of flow separation.

Arnold [9,10] used both a coupled panel/IBL method and RANS to compute the take-off and landing configurations. The IBL method agreed fairly well with surface pressures and integrated forces at lower angles, but overpredicted maximum lift. RANS solutions on a grid with 105,000 points and the Baldwin–Lomax turbulence model underpredicted lift and overpredicted drag. It also predicted wake vortices over the flap, which were believed to be unrealistically large. Use of a $k-\omega$ model improved results considerably.

Larsson [88] computed the take-off case using a $k-\varepsilon$ turbulence models with a structured-grid RANS code and transition points set according to experiment. The grid had 88,000 points. Surface pressures and skin friction at $\alpha = 12.2^\circ$ agreed well with experiment. The integrated forces and moments differed from experiment by $<5\%$. The far field circulation correction in the boundary condition [163] was necessary to obtain the correct drag level.

Lorentzen and Lindblad [95] used RANS with several turbulence models to compute the take-off configuration on a structured grid with 55,000 points. A $k-\varepsilon$ model predicted abrupt stall (different in character from the gradual stall seen in the experiment). Also, velocity profiles using the $k-\varepsilon$ model tended to exhibit the largest differences from experiment, particularly deeper wakes. Three variants of $k-\omega$ models, including a nonlinear explicit algebraic Reynolds-stress model, fared better. In particular, the angle of attack for maximum lift (and the gradual stall character) was captured. Lift and drag levels were in reasonable agreement with experiment. Surface pressure coefficients were in good agreement with experiment, and velocity profiles were in fair agreement. The numerical scheme and transition points were found to have a larger impact on the solution than the choice of turbulence model. The authors believed that the accurate computation of shear layer merging was a key to predicting $C_{L,max}$ at the correct angle of attack.

Thibert et al. [162] used an incompressible decoupled Navier–Stokes system plus panel method to compute both the take-off and landing configurations. The method did not account for wake/boundary layer merging. In the absence of flow separation, pressure

distributions were computed in fair agreement with experiment.

Lindblad and de Cock [92] summarized the results from the GARTEUR organization's validation exercise with this airfoil. Mainly the take-off configuration was considered, and most of the participants used RANS. A common structured grid with 55,000 points was supplied, although many participants used their own grids. Most of the RANS results agreed with each other and with experiment at lower angles of attack. Near maximum lift, there was considerable variation, with most methods underpredicting $C_{L,max}$. All turbulence models were two-equation models; overall, they gave fairly consistent results. The largest differences may in fact have been due to differences in transition or in numerical implementation. Most surface pressure predictions agreed well with experiment, but there was a considerable amount of spread in velocity profiles. Most methods tended to predict too deep a slat wake. Some unstructured-grid RANS results were also presented. They performed well, in general, but the boundary layer and wake profiles were less well resolved than on the structured grids.

To summarize results for the GARTEUR A310 3-element configuration:

- For this attached flow, most CFD methods gave surface pressures that were in very good agreement with experiment.
- Computing maximum lift was problematic: an IBL method overpredicted it, and most RANS methods tended to underpredict it.
- CFD tended to predict too pronounced a slat wake.
- There tended to be less effects due to turbulence model than due to transition and numerics.
- Drag was sensitive to the far field grid extent and/or boundary condition.
- Grid study validations were not reported.

4.4. MDA 3-element

Several of the most computed multi-element configurations have been various MDA three-element configurations, tested over the course of many years (primarily the 1990s) in the NASA Langley LTPT. The pressurized tunnel uses side-wall venting to achieve as 2-D a flow field as possible, as judged by spanwise pressure variations. Although several different configurations have been computed, this section will focus primarily on the 30P-30N rigging with both slat and flap deflected 30° (also referred to as geometry A), typical of a landing configuration. Therefore, not all references given in Table 3 are mentioned here. The Reynolds number in the tests varied from 5 to 16 million; most computations were performed at $Re = 9$ million. On the 30P-30N configuration, stall is not accompanied by any significant regions of separation on the upper surfaces of the elements.

Anderson et al. [4] used unstructured-grid RANS on a grid with over 87,000 points on the finest grid. They computed two Reynolds numbers as well as two flap configurations. By performing a grid sensitivity study, they showed that surface pressures were adequately resolved with 50,000 points, but that velocity profiles at high angles of attack required more. Trends due to Reynolds number and rigging changes were captured well, but the angle of attack for maximum lift was overpredicted.

Besnard et al. [21,22] used an IBL method to compute the 30P-30N at $Re = 9$ million. Transition was predicted by their method. Results agreed well with the experiment, although the lift tended to be slightly overpredicted. They also investigated the effects of flap gap, flap deflection, and Reynolds number. For moderate variations of the parameters, the overall trends were captured well.

Cao et al. [32] used an incompressible RANS solver with structured grids ranging from 65,000 to 280,000 points. The SA turbulence model included a rotation term to account for possible streamline curvature effects. Some of their conclusions were as follows. The grid effect was found to be small for pressure and skin friction distributions, but made a difference in the predicted velocity profiles. The inclusion of a point vortex model in the far field boundary condition [163] was deemed important for far field grid extents $< 40c$. Specifying transition location using experimentally determined locations yielded better results than using a transition-prediction capability. Finally, inclusion of tunnel walls (and the accurate vertical placement of the airfoil within the tunnel) in the CFD computation was found to be increasingly important at higher angles of attack. In comparison with the experiment, lift tended to be overpredicted near $C_{L,max}$. However, the authors noted that spanwise flow two-dimensionality was not achieved in the wind tunnel near maximum lift. Velocity profiles were in reasonable agreement with experiment, although the slat wake tended to be predicted too wide and deep. This slat wake disagreement was more pronounced when using the coarser grids.

Czerwiec et al. [42,43] used a structured-grid RANS code with a two-equation turbulence model and built-in transition prediction capability to compute the 30P-30N on a grid with over 135,000 points. In general, the model did a good job predicting the transition onset compared to experimentally measured locations. Surface pressure coefficients at $\alpha = 8°$, 16°, 19°, and 21° agreed well with experiment, and velocity profiles showed reasonably good agreement, although the slat wake was usually predicted to be too wide and too deep. The computed flow field at $\alpha = 21°$ showed evidence of unsteadiness.

Turbulent shear stress predictions showed fair agreement with experimental levels.

Dominik [47] used an incompressible structured-grid RANS code with three turbulence models: BB, SA, and SST. Fully-turbulent computations were employed. Through a grid-sensitivity study, a grid with over 118,000 points was deemed sufficient to predict trends. Surface pressure coefficients agreed well with experiment, but the angle of attack at maximum lift was consistently overpredicted. The BB model predicted the performance changes due to both rigging and Reynolds number changes, but SA and SST did not. The author noted that in Valarezo and Mavriplis [169], the SA model in a different code successfully predicted performance changes due to rigging. The reason for these opposing conclusions was unknown.

Jones et al. [73] predicted variations with Reynolds number and flap position well with a structured-grid RANS code and the SA turbulence model (fully turbulent). A grid with over 106,000 points included wind tunnel walls. Lift was consistently overpredicted, primarily over the main element, and velocity profiles showed prediction of the slat wake to be too wide and deep compared with experiment. Need for better grid distribution near the main element leading edge region was cited as a possible reason for overprediction of lift.

Kalitzen [74] used two structured-grid RANS codes and a grid with 135,000 points. Two turbulence models—SA and a 3-equation model—predicted similar velocity profiles at $\alpha = 19^\circ$. The slat wake was predicted too wide and deep compared to experiment.

Liou and Liu [93,94] used a structured-grid RANS code with SST and $k-\varepsilon$ turbulence models to compute the 30P-30N on a grid with 103,000 points. Using a built-in transition prediction methodology, transition was predicted in good agreement with experiment. Velocity profiles using the $k-\varepsilon$ model looked generally good, except that the slat wake was offset too far away from the main element, and appeared to be underresolved.

Lynch et al. [98] used an unstructured-grid RANS code with the SA turbulence model. Citing previous grid studies, they employed a grid with approximately 100,000 points. Some of the conclusions follow. The overall character of flow breakdown believed to be responsible for limiting the maximum lift was adequately captured by CFD, but at a higher angle of attack than experiment. The $C_{L,max}$ and angle of attack at which it occurred was overpredicted. The predicted wake spreading and deficit were too large in the CFD, especially for the slat wake. When increasing the flap gap, CFD did not capture the lift loss observed at lower approach-condition angles of attack, but predicted the ΔC_L trend near maximum lift. However, this result may have been fortuitous because CFD did not show reduced main wake size and consequent lowering of flap displacement thickness. When increasing the flap deflection, CFD missed the experimentally-measured trends at all angles of attack. Overall, the authors believed that the SA turbulence model was not adequately capturing the 2-D physics of importance for this flow field.

Morrison [108] investigated the effects of several numerical parameters and different turbulence models on the 30P-30N velocity profiles at $\alpha = 19^\circ$, using a structured grid with over 135,000 points and a RANS code. The flow was computed fully turbulent. Using spatially first-order vs. second-order advection in the $k-\omega$ turbulence model on the fine grid yielded minor differences in the region near the lower edge of the slat wake (first order was more diffused). Full Navier–Stokes vs. thin layer yielded very small differences. Use of an approximate production term for $k-\omega$, as opposed to the exact term, tended to reduce the slat wake deficit and generally diffused other regions of the velocity profiles. Two different versions of a $k-\varepsilon$ based EASM gave very similar results. Finally, in comparing three different turbulence models—standard $k-\varepsilon$, EASM $k-\varepsilon$, and $k-\omega$—results were generally similar, with EASM $k-\varepsilon$ giving too thick a boundary layer and a deeper slat wake deficit than the others. All three models overpredicted the slat wake width and depth.

Potter et al. [126] used two unstructured-grid RANS codes with the SA model (fully turbulent) on a grid with over 48,000 points. Surface pressure coefficients using the two codes agreed with each other and with experiment, but velocity profiles showed some differences. Lack of grid resolution in the wake regions resulted in overdissipated wake profiles with both codes, with the central-difference code showing more dissipation than the upwind code.

Rogers et al. [132,136] computed this configuration using an incompressible RANS code and various grids ranging from 54,000 to 213,000 points. Detailed guidelines were given for grid density and grid distribution. At high angles of attack, grid dependence in computed velocity profiles still existed between grid sizes of 83,000 and 213,000 points. Use of several different turbulence models—BB, SA, SST, and a new one-equation model—all tended to overpredict lift, particularly at angles of attack near $C_{L,max}$. The angle of attack for maximum lift was also generally overpredicted. (It is interesting to note that results for a slightly different MDA configuration using SST in Rogers [130] indicated a $C_{L,max}$ in relative agreement with experiment. This result is different from Rogers et al. [132] for the 30P-30N, in which SST results followed the same trend of overpredicting $C_{L,max}$ as other turbulence models.) Predicted surface pressures and skin friction were generally very good. Velocity profiles were predicted similarly using all turbulence models; all tended to overpredict the width and depth of the slat wake. For the most part, correct trends in lift were predicted for changes in the flap gap

and in the Reynolds number. In general, differences between predictions of different turbulence models were smaller than differences between CFD and experimental data.

Rumsey et al. [138,139] primarily focused on the effect of transition and turbulence model for the 30P-30N configuration using a structured-grid RANS code and a grid with over 135,000 points. Four turbulence models were employed: SA, SST, and a nonlinear EASM in $k-\varepsilon$ and $k-\omega$ forms. Surface pressure coefficients were predicted in good agreement with experiment. Transition locations on the elements were shown to have a large effect on predicted velocity profiles. Setting transition to match experimentally-measured locations improved boundary layer profiles considerably, but the slat wake was still predicted too wide and deep, regardless of the turbulence model employed (Fig. 8). By delaying transition on the slat to occur downstream of where it was observed, computed slat wake profiles better matched the experiment. The $k-\varepsilon$ form of EASM was shown to be ill-suited for use in this flow field because the ε equation performs poorly in regions of adverse pressure gradient wall-bounded flow. Nonlinear terms, present in EASM, improved the prediction of turbulent shear stress behavior behind the main element trailing edge (Fig. 9), but had little effect on the mean flow field. Curvature corrections for both SA and EASM (termed SARC and EASMCC) were investigated, and were found to have little effect in the region over the flap where curvature effects should be significant (see Fig. 9). Other than the $k-\varepsilon$ model, all turbulence models behaved similarly. The $C_{L,max}$ and the angle of attack at which it occurred was consistently overpredicted by all turbulence models (Fig. 10).

Valarezo and Mavriplis [169] used an unstructured RANS code on grids with 50,000–230,000 points. Using the SA turbulence model, lift was overpredicted, particularly near $C_{L,max}$, although surface pressures generally agreed well with experiment. The finer grid with 230,000 nodes predicted trends due to Reynolds number and flap gap better than a coarser grid. Velocity profiles agreed reasonably well with experiment, and were found to be dependent on dissipation levels set in the code. On the fine grid with low dissipation levels, the slat wake width and depth were predicted to be slightly too large. The flow through the flap well was investigated using three different turbulence models: SA, BB, and $k-\varepsilon$. All models were in closer agreement to each other than to experiment; all underpredicted the location of the attachment point.

Ying et al. [185] used a structured-grid RANS code on a grid with over 135,000 points and the SA turbulence model to investigate several aspects of this flow field. Some of the conclusions follow. The CFD maximum lift occurred at $\alpha = 23^\circ$ when flow over the slat reached the compressibility limit: the slat boundary layer separated

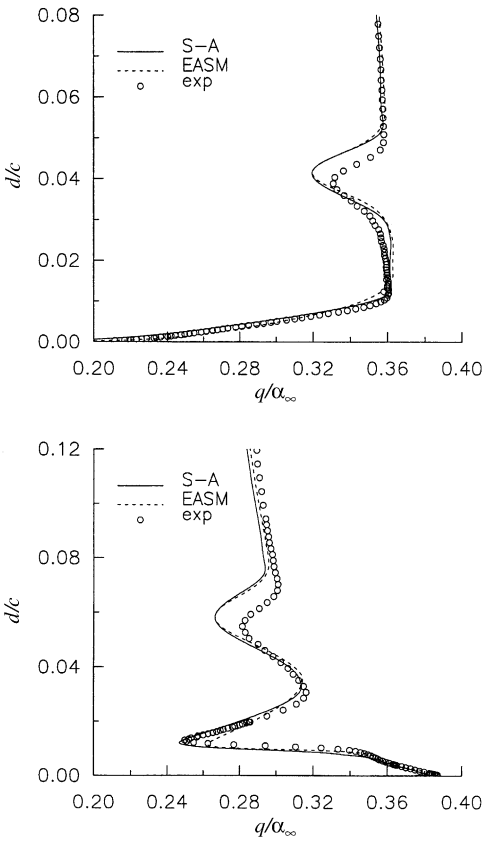

Fig. 8. Velocity profiles for the MDA 30P-30N airfoil, $\alpha = 19^\circ$; (a) $x/c = 0.45$, (b) $x/c = 0.89817$. Reprinted from Rumsey et al. [139].

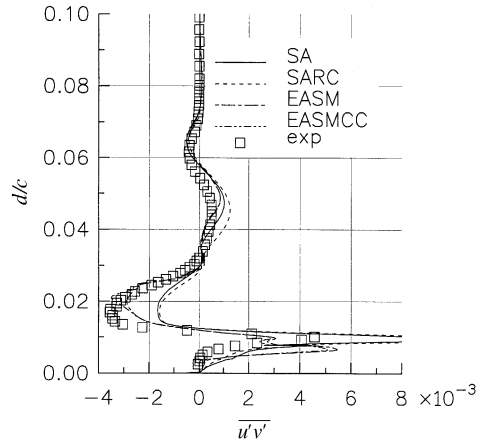

Fig. 9. Turbulent shear stress profiles on flap just downstream of main element for the MDA 30P-30N airfoil. Reprinted from Rumsey et al. [138].

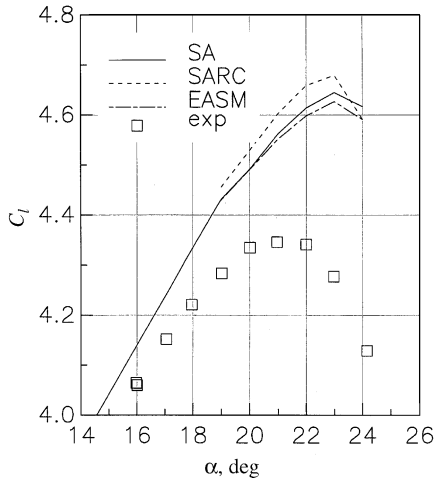

Fig. 10. Lift coefficients near maximum lift for the MDA 30P-30N airfoil. Reprinted from Rumsey et al. [138].

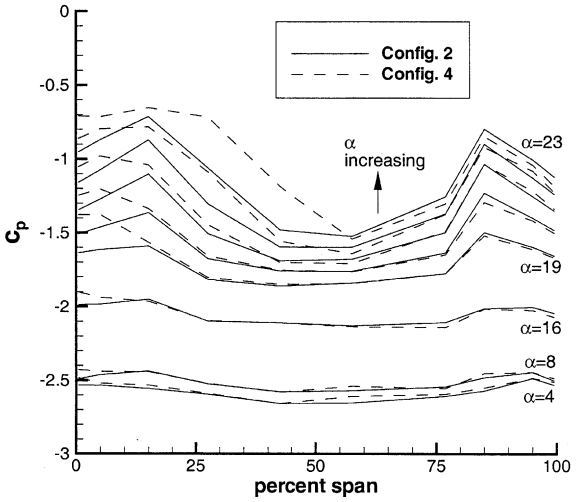

Fig. 11. Experimental spanwise surface pressure coefficients on the flap upper surface of the MDA 30P-30N, $x/c = 0.925$. (Config. 2 and 4 represent different side-wall venting configurations.) Reprinted from Rumsey et al. [140].

over a small region near its leading edge, and the resulting thickened slat wake caused the main element to stall because of momentum displacement. CFD successfully captured the Reynolds number effect at $\alpha = 19^\circ$ (between 5 and 9 million), but did not adequately capture the effect due to a flap gap change at the same angle of attack. The eddy viscosity assumption inherent in SA (and most other turbulence models in use today) was the source of disagreement in turbulent shear stress profiles aft of the main element trailing edge. Finally, some issues concerning coordinate frame of reference when comparing turbulent shear stress profiles were raised.

The 30P-30N configuration was the subject of a CFD challenge sponsored by NASA Langley in 1993, as reported by Klausmeyer and Lin [82]. Many methods and turbulence models were employed, and no standard grid was used. In general, RANS showed less variability than coupled IBL methods, although the coupled methods tended to predict drag better. It was recognized that use of a far field circulation correction [163] was necessary to predict drag better with the RANS codes when the grid outer boundary did not extend far enough. Lift was generally predicted high, and most codes predicted the angle of attack of maximum lift much later than experiment. Pressure and skin friction comparisons were very favorable overall, but there was a large variability in velocity profiles. The slat wake tended to be predicted as too large. The CFD methods generally captured changes due to Reynolds number, but not due to flap gap. Transition location was identified as a major flow physics issue: it was considered as a key to improved CFD modeling of this type of flow field.

Finally, we close this section with a discussion of recent work by Rumsey et al. [140]. This reference is different from the others described above in that it computed the nominally 2-D 30P-30N flow field using 3-D RANS, rather than 2-D RANS. The side-wall suction used in the LTPT experiment was also modeled. Both a structured grid with 4.47 million points and an unstructured grid with 1.35 million points were used in two different codes. The SA turbulence model was employed. In this combined experimental/computational paper, the focus was to try to determine if 3-D effects were a primary reason for disagreement between previous CFD computations and experiment near maximum lift for this configuration.

Fig. 11 shows spanwise surface pressure coefficients at $x/c = 0.925$ on the flap upper surface as a function of angle of attack in the experiment. (Two configurations shown are for different side-wall venting patterns near the flap.) Clearly, there was a significant amount of three-dimensionality in the flow field at angles of attack above $\alpha = 16^\circ$. Compare this figure with CFD results in Fig. 12. With the side-wall venting model, the CFD maintained better two-dimensionality than the experiment at all angles of attack up to the computed $C_{L,max}$, which in this case occurred at $\alpha = 21^\circ$. At $\alpha = 22^\circ$, an off-body vortex near the side wall increased in size, causing the increased spanwise variation seen in the figure, and hence decreased lift. Corresponding 2-D C_p levels are also shown in the figure; the 3-D levels on the flap differ slightly from the corresponding 2-D levels at and above an angle of attack of $\alpha = 16^\circ$, even though there is little spanwise variation.

Computed vs. experimental lift coefficients are shown in Fig. 13. 2-D CFD results are shown in this figure

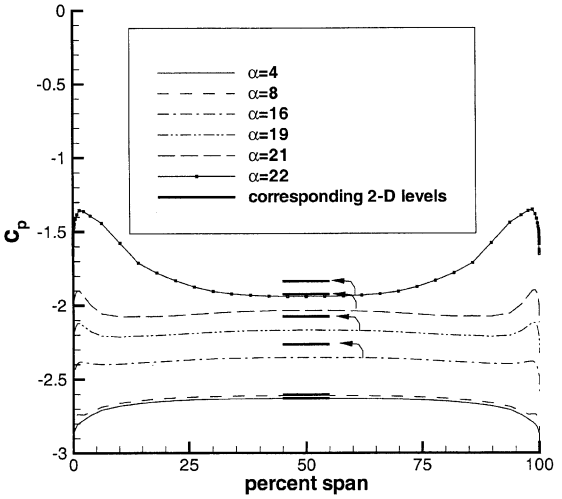

Fig. 12. Computed spanwise surface pressure coefficients on the flap upper surface of the MDA 30P-30N, $x/c = 0.925$. Reprinted from Rumsey et al. [140].

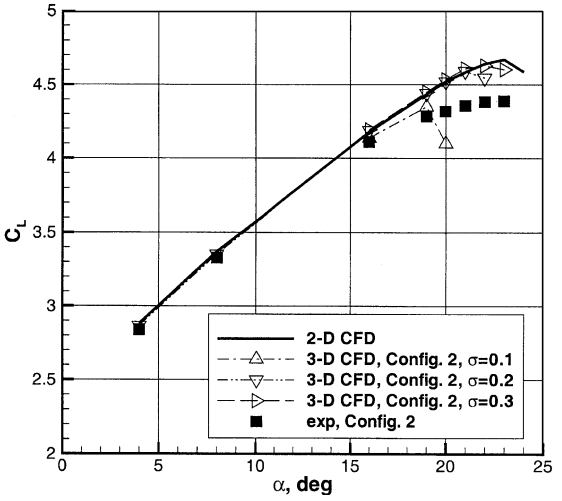

Fig. 13. Lift coefficients for the MDA 30P-30N. (Config. 2 represents a particular side-wall venting configuration, and σ represents the suction level.) Reprinted from Rumsey et al. [140].

along with 3-D results using three different suction levels, represented by the parameter σ. The larger σ, the larger the side-wall suction and the closer the 3-D calculations mimicked 2-D results. Using the smallest suction level of $\sigma = 0.1$, the CFD results appeared to be approaching the experiment, but the CFD stalled too early. This early stall was possibly due to under-resolution of the side-wall vortex which occurred near the wall at high angles of attack. (Note that the stall angle in the experiment using side-wall venting config. 2 in Fig. 13 is higher than the experimental stall angle of

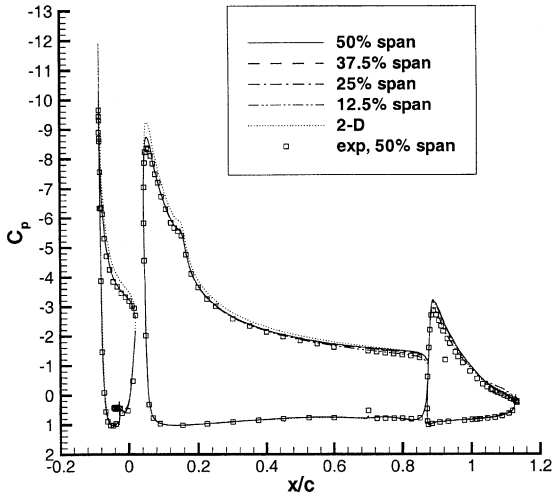

Fig. 14. Chordwise surface pressure coefficients for the MDA 30P-30N with no venting, $\alpha = 16^\circ$. Reprinted from Rumsey et al. [140].

$\alpha = 21^\circ$ using other venting configurations or that shown in Fig. 10 from an earlier test. This sensitivity is discussed in Rumsey et al. [140].)

Although the 3-D computations were unable to accurately model the experiment near maximum lift, they predicted the flow well both with and without side-wall venting at lower angles of attack. For example, Fig. 14 shows surface pressure coefficients at $\alpha = 16^\circ$ with no venting in either the experiment or the CFD. CFD generally agreed well with experiment. Notice that upper surface pressures on the slat and main elements were different from 2-D levels, due to reduced circulation caused by large side-wall interactions. Also, spanwise variations were evident in the CFD results near the trailing edge of the main element and on the flap. Fig. 15 shows results with venting. Again, CFD compared well with experiment, and this time the pressure levels generally agreed with 2-D levels, and there was no noticeable spanwise variation.

Brackets were included in unstructured-grid computations, and were found to reduce the lift levels near maximum lift by 2–3% ($\Delta C_L = 0.1-0.2$), although not enough to fully account for the excessive lift present in the structured-grid solutions. Deviations in the streamlines at high-lift conditions caused by the flap brackets can be seen in Fig. 16.

Some of the conclusions from Rumsey et al. [140] were that 3-D effects were significant in the experiment near maximum lift conditions, so 2-D CFD methods should not be expected to predict it. 3-D CFD was believed to be required to match such conditions, but grid resolution beyond what was used in this reference was needed. This research also indicated that faithful modeling of all walls and mounting hardware may be

necessary, because these features appear to have an increased impact near maximum lift conditions.

To summarize results for the MDA 3-element configuration:

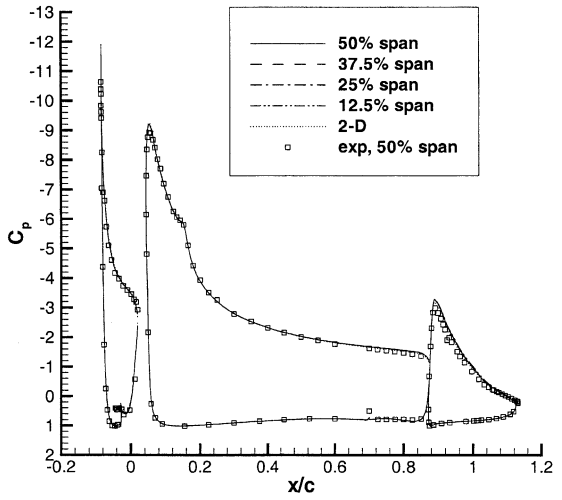

Fig. 15. Chordwise surface pressure coefficients for the MDA 30P-30N with venting, $\alpha = 16^\circ$. Reprinted from Rumsey et al. [140].

- For this attached flow, most CFD methods gave surface pressures that were in very good agreement with experiment.
- The angle of attack for $C_{L,max}$ was usually over-predicted.
- CFD tended to predict too pronounced a slat wake.
- Results using most turbulence models, including more advanced nonlinear models, tended to be similar in predicting mean flow quantities. However, the $k-\varepsilon$ models generally performed worse than others.
- Transition effects were important at the *Re* tested, and their locations could be reasonably well predicted by several different methods.
- Trends due to Reynolds number were generally predicted well, but trends due to rigging changes were inconsistent.
- Including tunnel walls in 2-D computations was more important near maximum lift conditions.
- Curvature corrections did not have a significant effect on results.
- Drag was sensitive to the far field grid extent and/or boundary condition.
- The experiment was increasingly 3-D as the angle of attack approached maximum lift; stall in the experiment may have been caused by 3-D effects in the wall-juncture region.

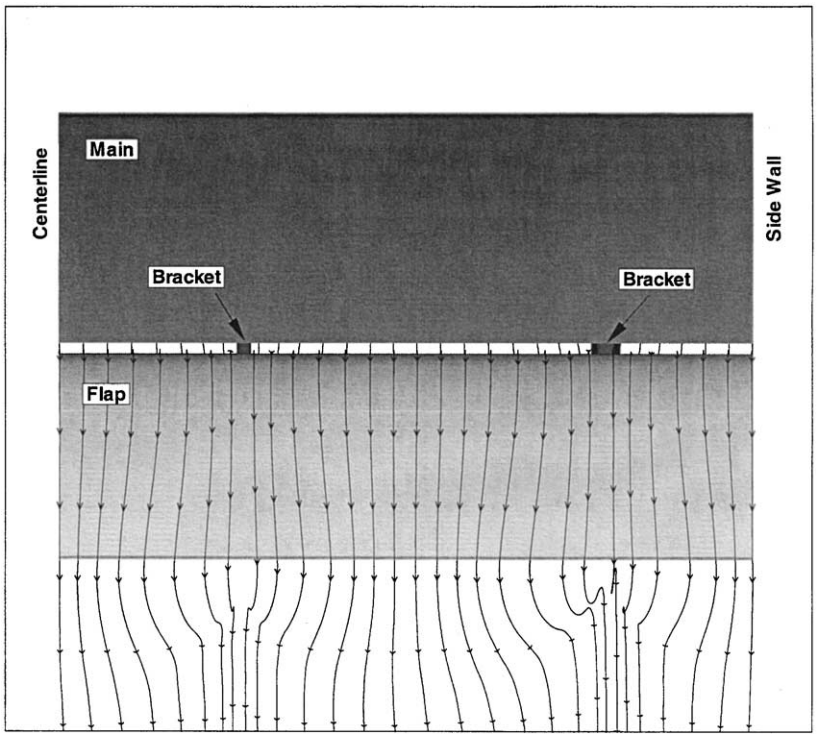

Fig. 16. Computed off-body streamlines for the MDA 30P-30N using unstructured method with brackets, looking upstream, $\alpha = 20^\circ$. Reprinted from Rumsey et al. [140].

- In the 2-D computations, grids with 50,000 points could adequately resolve surface pressures, but as many as 100,000–200,000 points were needed to resolve velocity profiles. The solutions were also sensitive to grid point distribution.

4.5. NHLP-2D 3-element

The NHLP-2D configuration was tested in the early 1970s as part of the UK National High-Lift Programme in the BAC wind tunnel. The Reynolds number was 3.52 million and side-wall suction was used in an attempt to maintain as 2-D a flow field as possible. Although double- and triple-slotted flaps were also tested, computations have only been performed on the 3-element (slat, main, and flap) configuration. Transition was fixed on the main element, but not on the slat or flap. Similar to the A310 and 30P-30N cases, stall does not occur due to massive separation on any of the elements. In the experiment, total pressure profiles were measured instead of velocity profiles.

Cebeci et al. [36] and Chang et al. [37] used a panel method coupled with an IBL approach. Surface pressure coefficients were predicted in good agreement with experiment, but angle of attack for maximum lift was significantly overpredicted. By artificially adjusting a constant in the turbulence model to cause a dramatic increase in the growth of the displacement thickness in the main element's wake, $C_{L,max}$ was better predicted.

De Rango and Zingg [45] used a higher order spatial discretization scheme in a structured-grid RANS code with the SA model to compute this flow field. Grids ranging from 52,000 to 255,000 points were used, and transition was specified in accordance with the experiment. Using a grid with 72,000 appeared to be sufficient to resolve velocity profiles using the higher order scheme, but not using the standard second-order scheme. Comparisons were not made with experimental total pressure profiles, but surface pressures were in good comparison with experiment.

Hussaini et al. [66] and Morrison [108] used a structured-grid RANS code on a grid with 115,000 points. Three different turbulence models were employed: $k-\varepsilon$, $k-\omega$, and a nonlinear EASM in $k-\varepsilon$ form. Transition locations were set on the main element according to the experiment, and the slat and flap were computed fully turbulent. Surface pressures agreed well with experiment at the two angles of attack $\alpha = 4.01^\circ$ and 20.18°. Total pressure profiles showed similar character to the experiment, but the slat wake depth was predicted to be too large. All three turbulence models yielded generally similar results. Using an empirical method to determine transition location on the slat resulted in some improvement, but the slat wake was still too deep. By artificially forcing the slat boundary layer to be laminar (rather than fully turbulent), the slat wake was predicted in much better agreement with experiment. It was noted that on the 115,000 point grid, the effect on velocity profiles of varying the order of accuracy of the turbulence model's advection term was significant, indicating that the grid was probably too coarse.

Nelson et al. [111] employed a structured-grid RANS code with the SA and SST turbulence models on a grid with 110,000 points. They set upper surface transition just aft of the minimum pressure on each of the elements. Computed forces and moments were in excellent agreement with experiment up to maximum lift, but it was necessary to set the transition point to be aft of laminar separation at $C_{L,max} = 22^\circ$ in order to accurately predict the lift at that angle of attack. Surface pressures and boundary layer total pressure profiles were in good agreement with experiment. The slat wake deficit and width were generally predicted in good agreement with experiment. Both turbulence models gave similar results.

Rumsey et al. [139] used a structured-grid RANS code with 115,000 points and three turbulence models—SA, SST, and EASM $k-\omega$—to compute the NHLP-2D configuration. Transition was set on the main element, whereas computations were fully turbulent on the slat and flap. The three turbulence models yielded overall similar results. In all cases, the slat wake was consistently predicted to be too deep. Lift and drag levels were in good agreement with experiment, but the angle of attack of stall was predicted to be too high (Fig. 17).

Wild [179] computed this flow using structured-grid RANS and a $k-\omega$ model within the context of an optimization methodology. At $\alpha = 20.18^\circ$, he showed the importance of accurate transition prediction for computing forces. There was not much of an effect on surface pressures, which generally agreed well with experiment.

The NHLP-2D case was the subject of a CFD challenge sponsored by the CFD Society of Canada in 1996, as reported by Fejtek [53]. There were ten participants representing a wide variety of methods. Standard grids were supplied, but not all participants utilized them. Overall, one of the conclusions was that the "official" grid consisting of 115,000 points was not fine enough, and another conclusion was that inconsistency among participants regarding transition specification made meaningful comparisons difficult. Incompressible RANS codes performed well at low angles of attack, but predicted drag less accurately at higher angles where compressibility was important. Also, these codes did not predict a $C_{L,max}$ at all. Compressible RANS codes generally performed well at all angles of attack, but $C_{L,max}$ was predicted too high by 1–2°. Using a grid extent of only $10c$, it was necessary to employ a circulation correction [163] to obtain reasonable drag levels. Surface pressures were generally

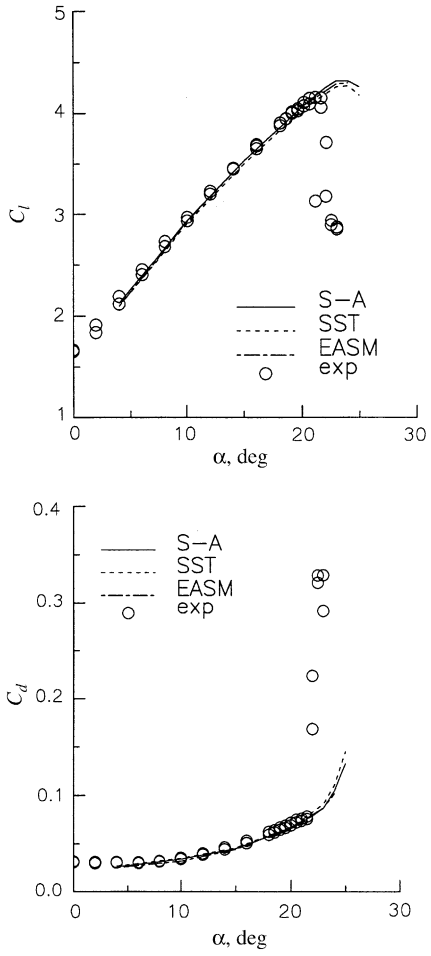

Fig. 17. Integrated force coefficients for the NHLP-2D airfoil; (a) lift coefficient, (b) drag coefficient. Reprinted from Rumsey et al. [139].

predicted well in comparison with experiment. The slat wake was generally displaced too far from the airfoil surface, and was generally predicted too deep. The slat transition location was found to significantly affect the downstream wake profiles. The effect of different turbulence models was generally small.

To summarize results for the NHLP-2D 3-element configuration:

- For this attached flow, most CFD methods gave surface pressures that were in very good agreement with experiment.
- The angle of attack for $C_{L,max}$ was usually overpredicted.
- CFD generally tended to predict too pronounced a slat wake.
- Different turbulence models tended to yield similar mean flow results.
- Transition location had a significant effect on results at the *Re* tested.
- The compressible RANS formulation gave better results than incompressible near maximum lift.
- Drag was sensitive to the far field grid extent and/or boundary condition.
- Grids on the order of 100,000 points were too coarse to fully resolve velocity profiles using globally second-order differencing schemes, but a grid with 72,000 points was adequate for a higher order scheme.

4.6. Omar 4-element

The Omar 4-element airfoil was tested in the Boeing research wind tunnel in the 1970s. Data was taken at $Re = 2.83$ million on several configurations, ranging from one element to five elements. Boundary layer control by means of tangential blowing on the side-wall turntables was used to maintain as 2-D a flow as possible. The double-slotted flap with slat configuration (4 elements) discussed here was termed model C. Boundary layer separation was present at some conditions.

Drela [49] used a coupled viscous/inviscid IBL method to solve for the flow field at $\alpha = 12.2^\circ$, close to the maximum lift point. He found that lift was limited by the bursting of the main element's wake over the primary flap. Computed surface pressures were in fairly good agreement with experiment.

Jasper et al. [70] used a structure-grid RANS code and the BL turbulence model. They did not report the grid size. Results at three different angles of attack showed generally good agreement with experimental surface pressures. The largest discrepancies occurred at $\alpha = 8.13^\circ$ on the vane element, where the CFD did not predict separation region present in the experiment.

Kusunose et al. [86] used a viscous/inviscid coupling code for this configuration, whose lower surface cove corner was removed to reduce numerical difficulties. Surface pressure coefficients were predicted in good agreement with experiment, although lift levels were overpredicted and the maximum lift point was off by approximately 2°. By fixing transition to be at the minimum pressure points (instead of "free", based on the e^9 method), lift levels were lowered, and the angle of attack of maximum lift was raised. These changes in trip location had a significant effect on the flap loadings.

Lyapunov and Wolkov [97] used a viscous–inviscid interaction model to compute forces and moment for this case. Lift was overpredicted at high-lift conditions.

Moitra [107] used an unstructured-grid RANS code and the SA turbulence model (fully turbulent). The grid size was not reported, but grid studies for other configurations used between 180,000 and 250,000 points. Lift as a function of angle of attack agreed well with

experimental data, including $C_{L,max}$ and the angle at which it occurred.

Finally, Rogers et al. [136] used a structured grid with approximately 55,000 points and an incompressible RANS code and BB to compute this flow. Similar results to Jasper et al. [70] were seen: surface pressures agreed with experiment in general, except at $\alpha = 8.13^\circ$ the amount of separation on the two flap elements was underpredicted.

To summarize results for the Omar 4-element configuration:

- It was difficult to compute the flow with separated conditions.
- Lift and $C_{L,max}$ were generally overpredicted, although the one RANS code that made a comparison predicted both well.
- Transition location had a significant effect on the results at the *Re* tested.
- Grid study validations were not reported.

4.7. Summary and key findings from 2-D cases

We now summarize the 2-D results discussed so far. Many of these conclusions have also been borne out in the other CFD studies for different configurations in Table 3 (not covered above). Wherever appropriate, we mention specific examples. While RANS methods have continued to make headway over the last decade, IBL methods clearly remain viable for the analysis of these types of flow fields. However, as a group, IBL methods tend to exhibit more variability than RANS methods (see [82]). This variability is probably due to the fact that IBL methods either miss certain physics altogether (such as wake effects or wake/boundary layer interaction) or else have code-specific built-in features or fixes to account for them. As a result, IBL codes taken as a group tend to be somewhat unreliable, but *specific* IBL codes have developed an impressive track record and remain valuable tools for design studies.

One of the biggest uncertainties associated with the use of RANS methods is the turbulence model. Through the 1990s there was a general shift away from algebraic turbulence models toward one-equation and two-equation linear models, as well as toward some more sophisticated nonlinear models. The algebraic models and "standard" two-equation models have been known to perform poorly for separated flows, and this trend still holds for separated multi-element airfoils (see also [39,143]). In particular, use of the ε-equation seems to be problematic for wall-bounded flows in adverse pressure gradient, which are a common feature in multi-element flow fields. Some of the other models developed in the 1990s—SA, BB, SST, and certain other variants such as nonlinear EASM—have generally improved predictive capabilities for separated flows. Among these models, differences between results for multi-element flows have tended to be relatively small for the most part (see also [46,65,75,77]), although details such as turbulent shear stress predictions are sometimes improved by using more complex models (see also [2]).

Transition, on the other hand, often has a relatively large effect on computed results for multi-element flows (see also [31,35]). Automatic determination of transition locations, begun in earnest in the early 1990s (see also [85]), has improved and continues to be a topic of active research today. At the very least, setting transition locations manually to match experiment appears to be a key ingredient to successfully predicting many measures of interest.

Not surprisingly, grid sizes tended to increase in density from $<50{,}000$ points to about triple this size as the decade advanced. Many independent grid studies seemed to suggest that 50,000 points may be sufficient to resolve surface pressures, but flow field quantities such as velocity profiles require significantly more (at least 100,000–200,000 points, unless a scheme with higher order spatial accuracy is employed). Grid issues overall tend to still remain very important. Those references that exercised the greatest care in ensuring high-quality, sufficiently-refined grids with an accurate representation of the wind tunnel geometry tended to produce the best correlations with experiment. Underresolution in key areas such as wakes can lead to overdissipation and incorrect conclusions. Also, for 2-D computations, it is important to have a far field grid extent of at least $50c$, or else special far field boundary condition treatment is required in order to accurately predict drag. Including tunnel walls in the computations appears to be increasingly important at higher angles of attack.

Incompressible RANS codes have been found to be less accurate than compressible RANS at high angles of attack, where sonic or near-sonic conditions can exist near the airfoil (see also [36,91]). However, even compressible CFD usually has had trouble predicting flows near maximum lift, with or without separated flow regions present. In general, the tendency has been for the lift and the $C_{L,max}$ to be predicted too high (see also [48,91]), but in certain cases the results have been the opposite (see also [51,86]), or have agreed well with experiment (see also [46,75,40]). A likely cause for much disagreement may be the fact that nominally 2-D experiments lose much of their 2-D character at high-lift conditions [140]. Comparing 2-D computations with 3-D high-lift flow fields may be too crude an approximation to yield meaningful comparisons.

Across the angle of attack range, RANS has generally been successful predicting trends due to Reynolds number (see also [85]), but has been less successful on the whole for trends due to configuration changes (see also [91]). Regarding specific flow field characteristics, the one that seems to stand out the most is the generally

poor prediction of the slat wake for several different configurations. Most RANS codes, regardless of turbulence model, tend to predict too pronounced a slat wake as it passes over the downstream elements (see also [17]). The cause of this poor prediction is still not known. Possibilities include poor modeling of transition effects, missing 3-D effects, turbulence models not capturing the relevant physics, and lack of unsteady slat cove effects. An experimental study on the 30P-30N configuration by Paschal et al. [120] showed organized structures ejected from the slat cove merging with the slat wake, but only at low angles of attack. No time-accurate CFD studies have been attempted to date to try to capture this type of feature.

It is difficult to obtain high-quality flow field measurement experimentally as far forward as the slat on these types of configurations, so the determination of precisely where and how the CFD goes wrong with regard to the slat wake has not yet been made. Carlson et al. [34] investigated the ability of a linear and a nonlinear turbulence model to predict wake development in zero, adverse, and favorable pressure gradient flows in a simple "unit problem" test. Both models predicted mean velocity profiles well, indicating their validity for predicting 2-D wake development. However, the (constant) gradients used in the study were smaller in magnitude than the (variable) gradients that occur on typical multi-element airfoils. So no firm conclusions are possible yet.

4.8. Summary and key findings from 3-D cases

Computations on 3-D high-lift configurations have been less prevalent and less organized than many of those for the 2-D configurations discussed above. Part of the reason for this difference is that the capability to perform adequate RANS computations on complex 3-D configurations has only really begun to emerge during the 1990s. Also, many of the configurations tested have been either of a preliminary or a proprietary nature, so conducting organized CFD "challenges" around such cases has not been possible. In this section, we summarize some of the capabilities and lessons learned from different isolated computational efforts on 3-D multi-element-type high-lift configurations, and attempt to draw some general conclusions at the end.

Baker et al. [12] used both incompressible and compressible structured-grid RANS codes with the SA turbulence model (fully turbulent) to compute flow over an unswept wing with half-span flap and either no slat, full-span slat, or three-quarter-span slat. Inviscid tunnel walls were modeled, and a careful study of tunnel outflow boundary conditions was conducted. Grid sizes ranged from 2.31 to 3.94 million points. Surface pressures agreed well with experiment. Although compressible regions were local to the slat and main element suction peaks, use of an incompressible code yielded significantly altered flow over the flap compared to a compressible code.

Berkman et al. [18] used a structured-grid RANS code with SA to compute the flow over a generic EET unswept wing configuration, with a focus on flap side-edge noise source identification. Two-element and three-element configurations were investigated. Grid sizes ranged from 4.8 to 5.7 million points, and included wind tunnel walls. Surface pressures agreed reasonably well with experiment at the angles of attack studied. Khorrami et al. [76] also focused on flap side-edge noise sources for a different part-span flap configuration using the same code and turbulence model. Grids (including wind tunnel walls) with up to 4.45 million points were used. Again, surface pressures agreed well with experiment at the angles of attack studied. Takallu and Laflin [159] used the same code and turbulence model to compute a part-span flap configuration tested in two different wind tunnels, with a focus on side-edge noise sources. Wind tunnel walls were modeled, and grids with 2.3–3.2 million points were utilized. Surface pressures agreed well with experiment.

Besnard et al. [21,20] used an IBL method to compute flow over the Lovell wing, a swept wing with slat and flap deployed. Modifications were made to the original Cebeci–Smith turbulence model. The need for an iterative wake shape calculation procedure was demonstrated, particularly for accurate stall predictions. Lift and drag were computed in good agreement with experiment when a certain wake shape was employed.

Cao et al. [33] computed flow over a 747PD high-lift configuration using a structured-grid RANS code with the SA turbulence model. Several configuration variations were tested, and some hardware (brackets, inboard engine strut and nacelle) were not modeled. Grid sizes ranged from 11.1 to 14.1 million points. Lift levels agreed well with experiment at low angles of attack. Near $C_{L,max}$, general performance trends were captured, but increments due to geometry changes (successive build-up from full-span Krueger, to Krueger with cutout and outboard strut, to Krueger with cutout and outboard strut and nacelle) were not. An assessment of grid effects was not performed, primarily due to the excessive time required to develop grids.

Corjon et al. [41] and Schonfeld et al. [141] performed Euler computations of the high-lift flow over an ALVAST wing-body configuration with deployed slat and flaps. The fine structured grid contained 3.5 million points. Because viscous terms were ignored, surface pressure results did not compare well with experiment. However, the focus of these works was on the accurate prediction of wake vortices, through a higher order spatial scheme with reduced dissipation. An unstructured-grid Euler code was also utilized on grids with 5.2 million elements (coarse grid) and 8.2 million elements

(fine grid). There was a clear enhancement in solution quality between the coarse and fine grids, but even on the fine grid the merging of outer flap end and tip vortices occurred too quickly.

Dutt and Jacob [50,68] used a 3-D inviscid lifting surface theory plus a 2-D analysis procedure (including boundary layer effects and a model for rear separation) to compute an unswept 3-element wing with flap separation. Surface pressures were in fair comparison with experiment.

Hyams et al. [67] computed the flow over an energy efficient transport (EET) configuration using an incompressible unstructured-grid RANS code and the SA model. The grid contained over 2 million points. Surface pressure coefficients showed reasonably good agreement with experiment.

Jones et al. [73] used a structured-grid RANS code and the SA model to compute flow over an unswept wing with full-span flap and part-span flap. Grid sizes were 1.47 and 2.79 million points, respectively. Both configurations yielded good comparisons with experimental surface pressures. There was qualitative agreement in the prediction of wake vortex locations (shed from the wing tip and flap tip), but the grids were not sufficiently dense to resolve the vortices adequately. Recall that in the 3-D computation of the 2-D 30P-30N flow field in Rumsey et al. [140], off-body side-wall vortical flow was also under-resolved by the grid (4.47 million points) at high angles of attack.

Mathias et al. [99] computed both full-span and part-span flap cases for an unswept wing using incompressible RANS with the BB model. Structured grids contained 900,000 points and 1.8 million points, respectively. On the full-span flap case, surface pressures agreed well with experiment, except that the experimental suction peak was somewhat stronger. No experimental comparisons were made for the part-span flap case.

Mavriplis [100] used an unstructured-grid RANS code with the SA turbulence model to solve the flow over an unswept part-span flap geometry. A grid with 1.7 million points was found to be too coarse to adequately predict the surface pressures; 13.5 million nodes yielded better comparisons. Mavriplis and Pirzadeh [101] also computed the flow over an EET high-lift configuration. A grid sensitivity study was performed, using two grids with 3.1 and 24.7 million points, respectively. There were relatively small differences in predicted surface pressures between the two grids. Both were in good agreement with experimental levels. Lift levels were slightly overpredicted, and the angle of attack for $C_{L,max}$ was overpredicted by 1° on the fine grid (Fig. 18). The drag coefficient was computed to within 10 drag counts (1 count = 0.0001) of the experiment over most of the operating range. Past stall, the steady computations failed to converge, producing variations in the forces

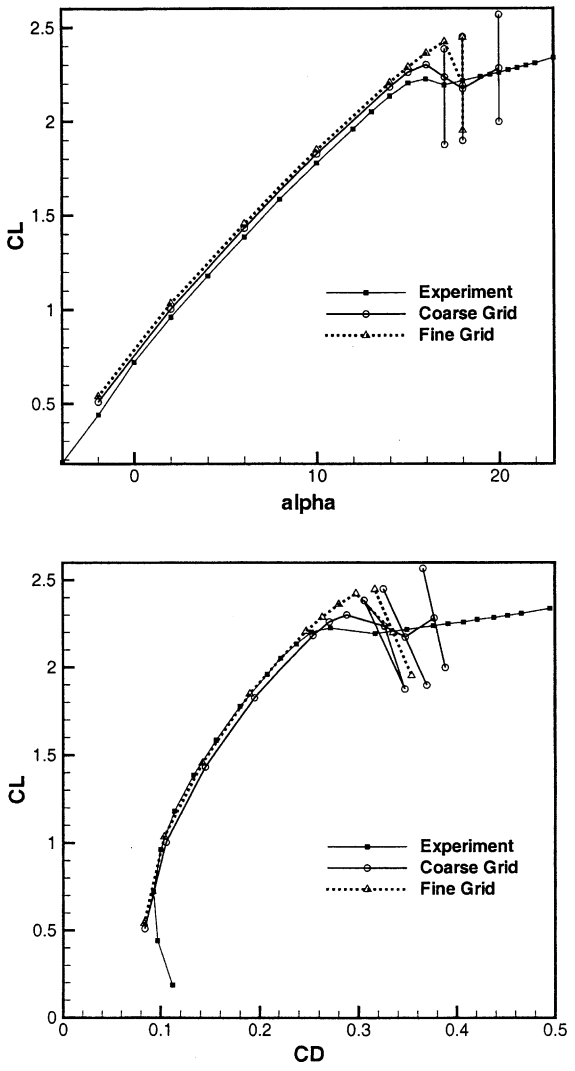

Fig. 18. Lift and drag coefficients for the EET configuration, from Mavriplis and Pirzadeh [101]. Copyright © 1999 by D.J. Mavriplis and S. Pirzadeh. Reprinted with permission.

whose mean followed the experimental levels. Preconditioning had very little effect on the results (preconditioned results were shown in the original figure in Mavriplis and Pirzadeh [101], but have been taken out of the figures here for clarity). Although the pressures and forces appeared to be grid-resolved, the authors believed that even the grid with 24.7 million points may have been too coarse in certain regions to capture particular flow features (for example, the slat wake).

Nash and Rogers [110] used a structured-grid RANS code with SA to compute the flow over a 3-element trapezoidal swept wing, including body pod. A baseline grid containing 6 million points was used, and grid refinement in individual coordinate directions yielded grids with up to 12 million points. Slat brackets were not

modeled. Three angles of attack of $\alpha = 20^\circ$, 33°, and 36° were computed. For the three finest grids, there was less than a 2% difference in C_L. However, surface pressures near the wing tip changed considerably, indicating the need for additional refinement in that region. The lift curve was in good agreement with experiment, except that the CFD predicted a rapid stall not seen in the experiment. There was overall agreement with experimental surface pressures, except at the outboard-most span station (98%), where predicted CFD sectional lift was too low.

Rogers et al. [133] computed the flow over the 777–200 aircraft in landing configuration using a structured-grid RANS code and the SA turbulence model. A total of 22.4 million grid points were used. The initial predicted lift was significantly low (by 11%) near maximum lift ($C_{L,max}$ was predicted too early). However, small differences in geometry between the CFD and experiment were shown to have significant effects on results. For example, a small gap between two elements caused local separated flow in the computations. In the experiment, this gap was partially sealed using wax and tape. When the grid was modified to better model this region ("sealed Krueger"), the predicted maximum lift increased by approximately 3%. Including a chine on the nacelle in the computations further increased the predicted maximum lift to be a total of 5% higher than the original grid system. The final computed C_L was within 1.5% and C_D was within 4% of experiment at approach conditions, and C_D also followed the experiment through maximum lift (Fig. 19). The $C_{L,max}$ was still significantly underpredicted. Surface pressures agreed well with experimental at lower angles of attack. At high angles of attack, the upper surface computed pressures were consistently higher than experiment.

Rogers et al. [134] computed the three-element trapezoidal wing with body pod using structured-grid RANS and the SA turbulence model. Grids were made for free air, inviscid wind tunnel walls, and high-fidelity viscous wind tunnel walls. These consisted of 6.0 million, 6.8 million, and 14.4 million grid points, respectively. Fig. 20 shows the configuration in the simplified tunnel. It was shown that including the wind tunnel walls was important, but approximating them as inviscid walls was sufficient. A global correction to angle of attack could be applied to free air results to obtain integrated force quantities in better agreement with experiment. However, local flow and relative loading of elements was likely to be different. Computed lift was slightly low (1° angle of attack offset) in comparison with experiment at low angles of attack, and deviated further near maximum lift. As expected, surface pressures followed this same trend. Spanwise grid refinement was applied to the grid in the inviscid tunnel, increasing the number of total points to 8.7 million. Although the refined grid was still not fine enough to remove grid dependencies, this

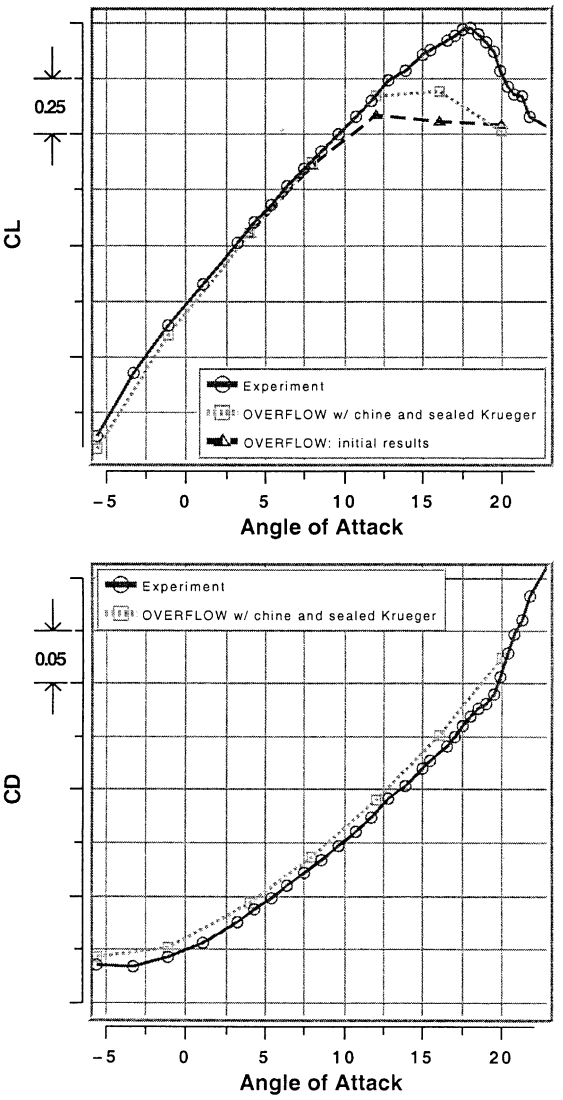

Fig. 19. Lift and drag coefficients for the 777–200 configuration, from Rogers et al. [133]. Copyright © 2000 by the American Institute of Aeronautics and Astronautics, Inc. Reprinted with permission.

change improved surface pressure comparisons at high angle of attack. However, instead of being underpredicted, $C_{L,max}$ (and the angle of attack at which it occurred) was overpredicted using the refined grid (Fig. 21).

Rudnik et al. [137] used both structured and unstructured-grid RANS codes to compute flow over the DLR ALVAST transport high-lift configuration. The structured-grid code used a $k-\omega$ model on a grid with 9.2 million points, and the unstructured-grid code used SA on a grid with 5.8 million points. Qualitatively, lift and drag were predicted to be generally in good agreement with the experiment, even near stall (Fig. 22).

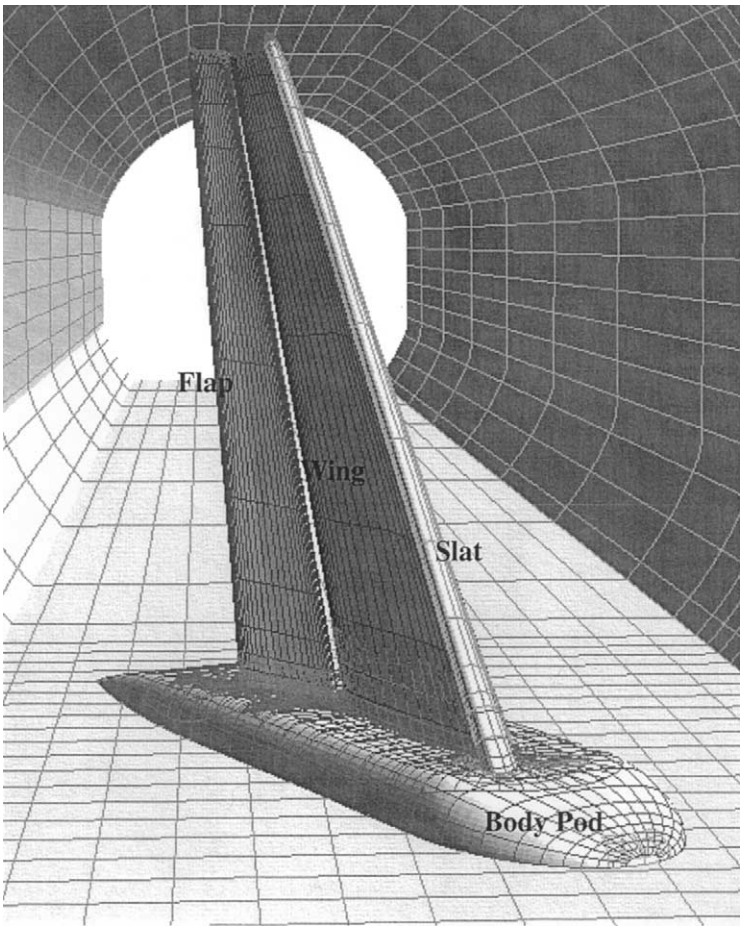

Fig. 20. Trap-wing surface grids inside simplified model of the 12-ft tunnel, from Rogers et al. [134]. Copyright © 2001 by the American Institute of Aeronautics and Astronautics, Inc. Reprinted with permission.

However, with the structured-grid code and $k-\omega$, too much separation was predicted at angles of attack above $\alpha = 15^{\circ}$, and lift was low by about 5%. The unstructured-grid code with SA tended to overpredict lift by 4.5%, even in the linear $C_L - \alpha$ range. It did not separate as much as the structured-grid computations at high-lift conditions. Except near stall, surface pressure coefficients agreed well with experiment. The influence of artificial dissipation and preconditioning was found to be small. It was noted that use of fully turbulent computations may have introduced differences from the experiment, in which transition regions were evident. Finally, there were some geometric differences between the CFD and experiment; in particular, the wind tunnel model had an endplate at the slat edge and a fairing between the wing upper surface and fuselage.

Slotnick et al. [144] used structured-grid RANS with SA to compute a high-wing transport high-lift configuration (both unpowered and powered). The grid contained 35.2 million points. Corrected experimental data was compared with free air computations, and uncorrected experimental data was compared with computations that included tunnel walls. As shown in Fig. 23, for the unpowered case ($C_{mu} = 0.03$), the computed lift and surface pressures (with or without walls) agreed very well with experimental data, even at $C_{L,max}$. (The numbers in the figure referred to specific conditions given in the reference; they have no meaning here.) Surface pressures agreed well with experiment. For the powered case ($C_{mu} = 0.5$), CFD did not capture the nonlinearity in lift curve slope. After analysis, it was concluded that the SA model's inability to model 3-D jet spreading and mixing was a primary cause for the disagreement. Other studies included an analysis of nacelle strake effectiveness, and of wake vortex prediction. In both cases there was qualitative agreement, but also some deficiencies: further grid refinement was warranted. For the wake vortex prediction, wind tunnel walls needed to be modeled.

Takallu [158] computed an EET wing-body configuration with a 4-element wing using structured-grid RANS and the SA turbulence model. Two grids

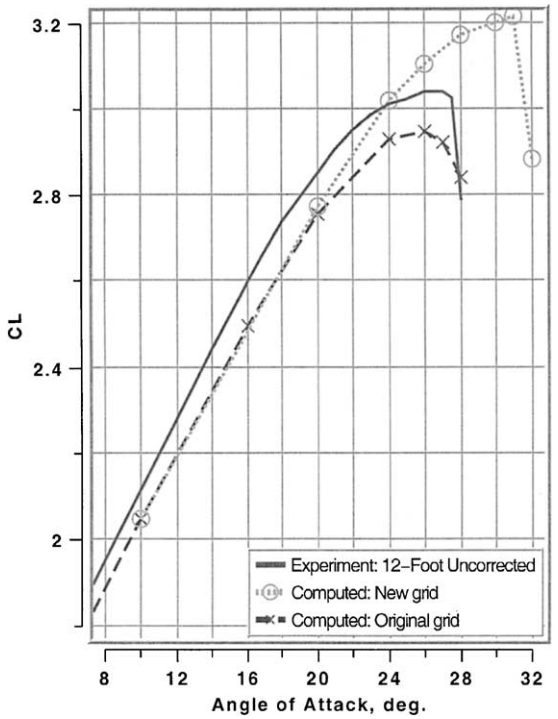

Fig. 21. Lift coefficients for the trap-wing configuration, from Rogers et al. [134]. Copyright © 2001 by the American Institute of Aeronautics and Astronautics, Inc. Reprinted with permission.

modeled the configuration both without and with a standoff from the wall, for 13.4 or 14.0 million points, respectively. Lift was predicted in excellent agreement with experiment through the lift break for both full-span and semi-span (with standoff) configurations; solutions were not obtained at higher angles of attack. Surface pressures also agreed well with experiment.

Valarezo and Chin [166] developed a semi-empirical method for determining $C_{L,max}$ for complex multi-element geometries. It used a surface panel method and a pressure difference rule (PDR) to predict maximum lift for several configurations, including an EET configuration. The method was also able to predict Reynolds number effect on $C_{L,max}$ surprisingly well.

In summary, similar to 2-D, some specific IBL methods in 3-D still have a place and are valuable tools for multi-element wing design. But 3-D RANS computations have begun to make some headway: they seem to generally be able to predict many complex multi-element flow fields at angles of attack below stall. However, their performance near maximum lift conditions has been less reliable, depending on the particular configuration. It is not easy to determine the precise causes for the differences. While it is possible that existing turbulence models fail to adequately represent the high-lift flow physics, the fact that the same model (SA) sometimes

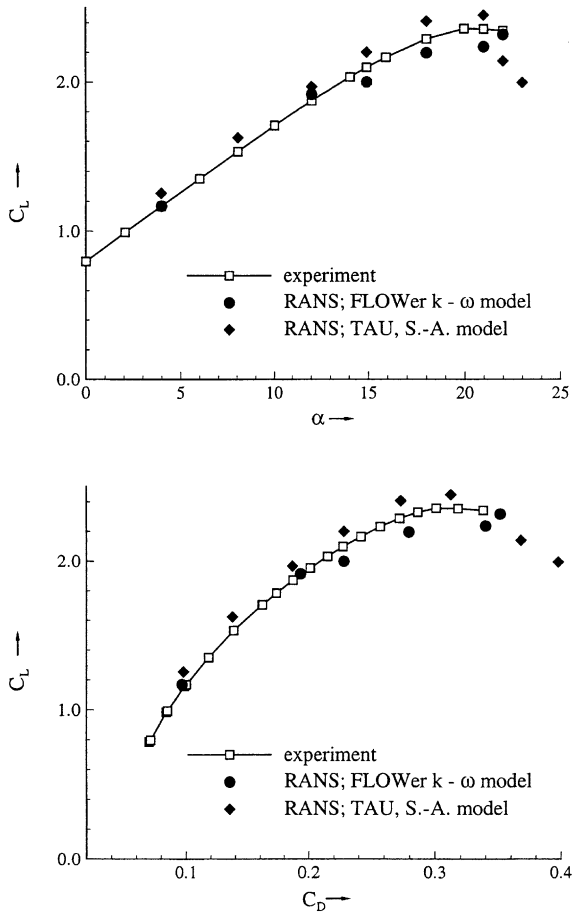

Fig. 22. Lift and drag coefficients for the DLR ALVAST configuration, from Rudnik et al. [137]. Copyright © 2001 by R. Rudnik, S. Melber, A. Ronzheimer, and O. Brodersen. Reprinted with permission.

does well and sometimes does not seems to indicate that the most significant influences lie elsewhere. It appears more likely that flow fields near maximum lift require more grid resolution and/or better geometric fidelity, the particulars of which are dependent on the configuration in question.

For 3-D configurations, detailed grid sensitivity studies are rarely performed due to excessive computational cost. And when they are, grid variation is often fairly limited or is only done in certain coordinate directions. This means that for most 3-D computational studies to date, insufficient grid resolution is an unaccounted-for possible source of error. It is interesting to note that even for the reference that used the finest 3-D grid (35.2 million points) [144], further grid refinement in certain regions of the flow field was still called for. Also, due to gridding complexity, it is often common practice to neglect some hardware, such as support brackets, when computationally modeling 3-D

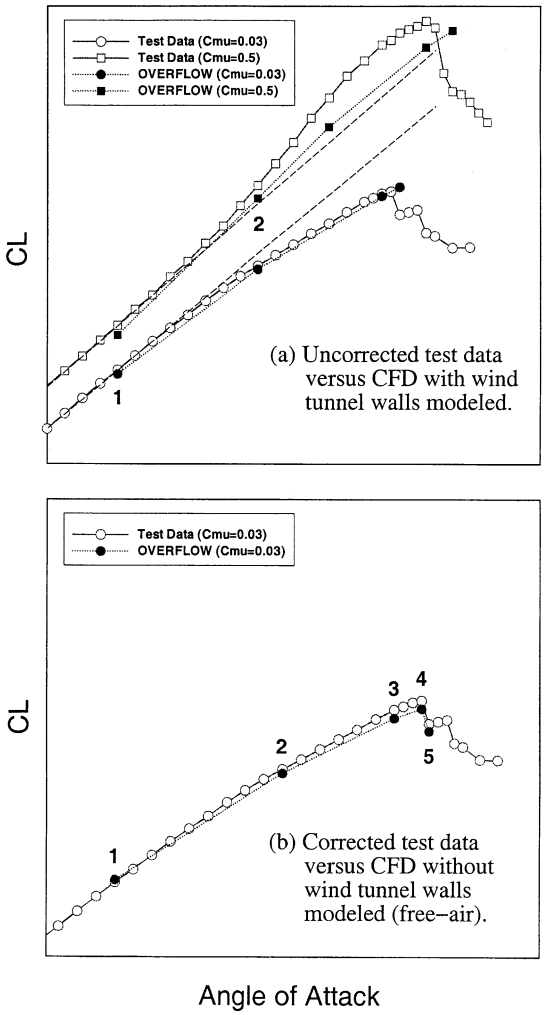

Fig. 23. Lift coefficients for the HWT configuration, from Slotnick et al. [144]. Copyright © 2000 by the American Institute of Aeronautics and Astronautics, Inc. Reprinted with permission.

configurations. By not faithfully representing all aspects of the configuration (especially small gaps and edges), some errors may be introduced, as was demonstrated by Rogers et al. [133].

For the most part, compressible RANS codes are preferred over incompressible for use on high-lift 3-D flows because such flows usually possess noticeable compressibility effects, which the incompressible formulation cannot handle. This lesson was also learned for 2-D flows.

Few 3-D studies have been conducted to date using different turbulence models. The SA model has generally been the most commonly employed. Furthermore, most 3-D studies have been run as being fully turbulent. Considering how important accurate specification of transition locations is for 2-D multi-element flows at typical wind tunnel *Re*, the same factor is also likely to be important in 3-D.

5. Conclusions and future challenges

The past 10–15 years have been a very active time for the application of computational methods to increasingly complex high-lift aerodynamic problems. As computer power has increased, so too has the range of problems attacked. Although less costly IBL methods remain an attractive and viable alternative for designing and analyzing multi-element configurations, RANS methods have been the focus of most of the research papers on this topic. Therefore, the majority of the specific conclusions listed below pertain to RANS methods.

Ultimately, aircraft designers need a reliable CFD tool that can accurately predict effects due to small configuration changes at high-lift conditions. Section 1.1 listed some possible reasons for inconsistent CFD predictions of high-lift flow fields. These were: (1) unsteady effects, (2) inadequacy of turbulence models, and (3) numerical errors and lack of geometric or modeling fidelity. Based on the results of the current review, it appears that number (3) probably plays the most dominant role at this point in time. Certainly, (1) and (2) may have an impact in particular flow field regions and at particular conditions, but choice of turbulence model (from among the best available) at least does not appear to have a *dominant* impact on mean-flow quantities in general. Given that nominally 2-D wind-tunnel flows near maximum lift probably possess three-dimensionality in spite of side-wall boundary layer control, 3-D CFD may be required to adequately represent such flow fields. Grid requirements for 3-D high-lift computations have yet to be firmly established.

The following is a summary of present CFD capabilities, as gleaned from the cited research papers. Note that the conclusions are based on research primarily conducted for $Re < 10$ million and at subsonic Mach numbers, so their validity cannot be presumed at other conditions.

1. In both 2-D and 3-D flows, surface pressures, skin friction, lift, and drag can generally be predicted with reasonably good accuracy at angles of attack below stall.
2. In 2-D flows, computed velocity profiles (with the exception of slat wakes) generally follow experiment reasonably well. Misprediction of the slat wake does not appear to have a significant influence on integrated quantities below stall. Not enough comparisons have been made yet in 3-D to know if the same trend regarding slat wake holds there.

3. In 2-D flows, trends due to Reynolds number can usually be predicted. However, analysis to date has only been performed at relatively low ($Re<10$ million) Reynolds numbers at which wind tunnel measurements have been available. Trends due to geometry changes (e.g., gap, overhang) can *sometimes* be predicted, but in general CFD is unreliable in this regard.

Caveats to the above capabilities are:

- For IBL methods, special treatment (such as modification of the turbulence model in the wake and iterative wake shape calculation procedure) must be included to account for wakes and wake/boundary layer interaction effects.
- For RANS methods, sufficient grid density must be employed (usually at least 50,000 points in 2-D for surface pressures and 100,000–200,000 points in 2-D for velocity profiles). There is no general guideline for 3-D established yet.
- Grid distribution is also an important factor: sufficient grid resolution is required in key areas of the flow field (e.g., wakes, vortices).
- Sufficient grid extent must be employed (at least $50c$ in 2-D), or else a modified far field boundary condition is needed. There is no general guideline for 3-D established yet.
- Transition locations should be comparable to those in the experiment.
- If there is separated flow, then one of the more recent turbulence models calibrated to perform better for separated flows (e.g., SA, SST, EASM) should be employed. There tends to be little difference between field-equation models of this type for mean-flow quantities in multi-element flows at these conditions.
- Some forms of the $k-\varepsilon$ two-equation turbulence model should be avoided for adverse pressure gradient wall-bounded flows.
- The configuration should be modeled as accurately as possible (e.g., support brackets, aeroelastic deformations, tunnel walls, chines), or else effects should be known. Accurate geometric fidelity appears to be more crucial as the angle of attack approaches maximum lift.

The following is a list of CFD (and experimental) challenges in the area of high-lift flows for the next decade. This list represents areas for which present CFD capabilities are deficient or where improved understanding is needed before significant CFD advances can be made.

1. Quantify what is required to consistently predict flow fields near maximum lift accurately using 3-D CFD. Many of the lessons to be learned here will come from additional collective experiences with a greater number of 3-D configurations, as well as continued advances in CFD methods such as adaptive grid techniques. Future "CFD challenges" involving quality 3-D high-lift datasets would contribute to this endeavor.
2. Obtain more experimental databases specifically for CFD validation. With computer capacity increasing, it is becoming easier to perform 3-D computations. With this in mind, it is important to document those aspects of wind tunnel experiments that must be modeled in 3-D computations, so that *all* CFD boundary conditions can be accurately defined. For example, in nominally 2-D experiments with side-wall boundary layer control, details about the flow through the side-wall must be available to CFD modelers. Also, more high-Reynolds number and flight test databases are needed.
3. Determine the cause for slat wake mispredictions by RANS (possibilities include poor modeling of transition effects, lack of unsteady effects, missing 3-D effects, and turbulence models not capturing the relevant physics).
4. Improve turbulent shear stress predictions. Unlike mean flow quantities, the turbulent shear stress can be dependent on the turbulence model employed in certain key regions of multi-element flow fields. Hence, this challenge involves continued methodical turbulence model development, refinement, and testing, particularly through the use of simplified "unit problems". Because transition and turbulence effects are interrelated, it also includes continued development of transition prediction capability.
5. Explore unsteady effects. Very little has been done to date in this area for multi-element high-lift flows, either computationally or in experiment.

Considering its capabilities 10–15 years ago, CFD has come a long way toward becoming a useful tool for the design and analysis of 3-D high-lift aerodynamic systems. The lessons learned from the many CFD studies conducted during the last decade should help to propel the field forward as it sets out to tackle the next series of high-lift challenges.

Acknowledgements

The authors gratefully acknowledge James Thomas and Veer Vatsa of NASA Langley for their comments and suggestions, and Dimitri Mavriplis of ICASE, Stuart Rogers of NASA Ames, Ralf Rudnik of DLR, Jeffrey Slotnick of Boeing, and David Zingg of the University of Toronto for their assistance in obtaining electronic copies of their figures.

References

[1] Adair D, Horne C. Turbulent separated flow over and downstream of a two-element airfoil. Exp Fluids 1989;7:531–41; Also NASA TM-100053, February 1988.

[2] Agoropoulos D, Squire LC. Interactions between turbulent wakes and boundary layers. AIAA J 1988;26(10):1194–200.

[3] Alexandrov NM, Nielsen EJ, Lewis RM, Anderson WK. First-order model management with variable-fidelity physics applied to multi-element airfoil optimization. AIAA Paper 2000-4886, September 2000.

[4] Anderson WK, Bonhaus DL, McGhee RJ, Walker BS. Navier–Stokes computations and experimental comparisons for multielement airfoil configurations. J Aircr 1995;32(6):1246–53; Also AIAA Paper 93-0645, January 1993.

[5] Applin ZT, Gentry Jr GL. Pressure distributions from subsonic tests of an advanced laminar flow control wing with leading and trailing edge flaps. NASA TM-4040, July 1988.

[6] Applin ZT. Pressure distributions from subsonic tests of a NACA 0012 semispan wing model. NASA TM-110148, February 1995.

[7] Arlinger BG, Larsson T. NLR 7301 two-element airfoil at high lift. In: Haase W, Chaput E, Elsholz E, Leschziner MA, Muller UR, editors. ECARP—European Computational Aerodynamic Research Project, validation of CFD codes and assessment of turbulence models. Notes on numerical fluid mechanics (NNFM), vol. 58. Braunschweig: Vieweg, 1997. p. 375–96.

[8] Arlinger BG, Larsson T, Arnold F, Earnshaw PB, Moens F, Saliveros E, Termes APP. Reynolds- and Mach-number effects and 2d–3d correlation based on measurements and computed results for the GARTEUR take-off configuration. High lift and separation control, Proceedings of the Conference, University of Bath, UK. London: Royal Aeronautical Society, 1995. p. 26.1–26.15.

[9] Arnold F. Numerical flow simulation on high-lift configurations at Daimier–Benz Aerospace Airbus. High lift and separation control, Proceedings of the Conference, University of Bath, UK. London: Royal Aeronautical Society, 1995. p. 8.1–8.9.

[10] Arnold F, Thiele F. LaPlace interaction law for the computation of viscous airfoil flow in low- and high-speed aerodynamics. AIAA J 1994;31(11):2178–85; Also AIAA Paper 93-3462, August 1993.

[11] Bailey R, Longo JMA, Radespiel R, Ronzheimer A, Demier A, Kroll N, Rossow C-C. Numerical calculations of high lift flows using structured and unstructured methods. AGARD CP-515, September, 1993. p. 14.1–14.13.

[12] Baker MD, Mathias DL, Roth KR, Cummings RM. Numerical investigation of slat and compressibility effects for a high-lift wing. AIAA Paper 99-0538, January 1999.

[13] Balasubramanian R, Jones KM, Waggoner EG. Assessment of computational issues associated with analysis of high lift-systems. Proceedings of the Fifth Symposium on Numerical and Physical Aspects of Aerodynamic Flows, California State University, Long Beach, CA, January 1992, Also NASA CR-193000, Part 1, January 1992.

[14] Baldwin BS, Barth TJ. A one-equation turbulence transport model for high Reynolds number wall-bounded flows. NASA TM 102847, 1990.

[15] Baldwin BS, Lomax H. Thin layer approximation and algebraic model for separated turbulent flows. AIAA Paper 78–257, June 1978.

[16] Bardina JE, Huang PG, Coakley TJ. Turbulence modeling validation, testing, and development. NASA TM 110446, April 1997.

[17] Bartsch P, Nitsche W, Britsch M. Navier–Stokes computations of turbulent flow around high-lift configurations. AGARD CP-515, September, 1993. p. 6.1–6.10.

[18] Berkman ME, Khorrami MR, Choudhari M, Sadowski SS. Investigation of high-lift flowfield of an energy efficient transport wing. J Aircr 2000;37(1):45–52.

[19] Bertelrud A. Transition on a three-element high lift configuration at high Reynolds numbers. AIAA Paper 98-0703, January 1998.

[20] Besnard E, Kural O, Cebeci T. Flow predictions about three-dimensional high lift systems. AIAA Paper 99-0543, January 1999.

[21] Besnard E, Puech B, Ivshin D, Kural O, Cebeci T. Prediction of stall and post-stall in two- and three-dimensional flows. AIAA Paper 2000-0979, January 2000.

[22] Besnard E, Schmitz A, Boscher E, Garcia N, Cebeci T. Two-dimensional aircraft high lift system design and optimization. AIAA Paper 98-0123, January 1998.

[23] Bonhaus DL, Anderson WK, Mavriplis DJ. Numerical study to assess sulfur hexafluoride as a medium for testing multielement airfoils. NASA TP 3496, June 1995.

[24] Braden JA, Whipkey RR, Jones GS, Lilley DE. Experimental study of the separating confluent boundary-layer, vol. I. NASA CR-3655, March 1983.

[25] Braden JA, Whipkey RR, Jones GS, Lilley DE. Experimental study of the separating confluent boundary-layer, vol. II. NASA CR-166018, March 1983.

[26] Brune GW, McMasters JH. Computational aerodynamics applied to high-lift systems. In: Henne PA, editor. Applied computational aerodynamics, progress in astronautics and aeronautics, vol. 125. Washington, DC: AIAA, 1990. p. 389–433.

[27] Brune GW, Sikavi DA. Experimental investigation of the confluent boundary layer of a multielement low speed airfoil. AIAA Paper 83-0566, January 1983.

[28] Burt M. A selection of experimental test cases for the validation of CFD codes: Chapter 5-summaries of the test cases. AGARD AR-303 vol. 1, 1994;August:55–133.

[29] Cantariti FJJ, Johnston LJ. High-lift Navier-Stokes computations on unstructured grids using a differential Reynolds stress model. In: Morton KW, Baines MJ, editors. Numerical Methods for Fluid Dynamics V. Oxford, UK: Clarendon Press, 1995. p. 319–25.

[30] Cantariti FJJ, Johnston LJ. Analysis of high-lift system aerodynamics using an unstructured flow solver and differential Reynolds stress modelling. Proceedings of the Seventh Biennial Colloquium on Computational Fluid Dynamics, University of Manchester Institute of Science and Technology, UK, May 1996. p. 3.7–3.8.

[31] Cao HV, Kusunose K. Grid generation and Navier–Stokes analysis for multi-element airfoils. AIAA Paper 94-0748, January 1994.

[32] Cao HV, Kusunose K, Spalart PR, Ishimitsu KK, Rogers SE, McGhee RJ. Study of wind tunnel wall interference for multi-element airfoils using a Navier–Stokes code. AIAA Paper 94-1933, June 1994.
[33] Cao HV, Su TY, Rogers SE. Navier–Stokes analyses of a 747 high lift configuration. AIAA Paper 98-2623, June 1998.
[34] Carlson JR, Duquesne N, Rumsey CL, Gatski TB. Computation of turbulent wake flows in variable pressure gradient. Comput Fluids 2001;30:161–87.
[35] Cebeci T. Calculation of multielement airfoils, wings at high lift. AGARD CP-515, September, 1993. p. 24.1–24.15.
[36] Cebeci T, Besnard E, Chen HH. An interactive boundary-layer method for multielement airfoils. Comput Fluids 1998;27(5–6):651–61.
[37] Chang KC, Chen HH, Tzong T, Cebeci T. Aeroelastic analysis of high lift configurations. AIAA Paper 2000-0905, January 2000.
[38] Chin VD, Peters DW, Spaid FW, McGhee RJ. Flowfield measurements about a multi-element airfoil at high Reynolds numbers. AIAA Paper 93-3137, July 1993.
[39] Chow R, Chu K. Navier-Stokes solution for high-lift multielement airfoil system with flap separation. AIAA Paper 91-1623, June 1991.
[40] Chow R, Chu K, Carpenter G. Navier–Stokes simulation of flow field around a blown-flap high-lift system. AGARD CP-515, September, 1993. p. 15.1–15.10.
[41] Corjon A, Darracq D, Champagneux S, Gacherieu C, Schoenfeld T. Simulation of aircraft in high-lift configuration. AIAA Paper 99-3179, June–July 1999.
[42] Czerwiec R, Edwards JR, Rumsey CL, Bertelrud A, Hassan HA. Study of high-lift configurations using k–ζ transition/turbulence model. J Aircr 2000;37(6):1008–16; Also AIAA Paper 99-3186, June–July 1999.
[43] Czerwiec R, Edwards JR, Rumsey CL, Hassan HA. Theory and experiment of multielement airfoils—a comparison. AIAA Paper 2000-0984, January 2000.
[44] De Cock K. High-lift system analysis method using unstructured meshes. AGARD CP-515, September, 1993. p. 12.1–12.20.
[45] De Rango S, Zingg DW. Higher-order spatial discretization for turbulent aerodynamic computations. AIAA J 2001;39(7):1296–304.
[46] Dodbele SS, Hobbs CR, Kern SB, Ghee TA, Hall DR, Ely WL. Wind tunnel experiments and Navier-Stokes computations of a high-lift military airfoil. AIAA Paper 99-0540, January 1999.
[47] Dominik CJ. Application of the incompressible Navier–Stokes equations to high-lift flows. AIAA Paper 94-1872, June 1994.
[48] Drela M. Newton solution of coupled viscous/inviscid multielement airfoil flows. AIAA Paper 90-1470, June 1990.
[49] Drela, M. Design and optimization method for multi-element airfoils. AIAA Paper 93-0969, February 1993.
[50] Dutt, HNV, Jacob K. Viscous subsonic flow computation for wings with flaps for high-lift. J Aircr 1993;30(1):141–3.
[51] Egami K, Shima E, Nakamura S, Amano K. Two-dimensional Navier–Stokes analysis of high-lift multi-element airfoils using the q–ω turbulence model. AIAA Paper 93-0679, January 1993.
[52] Eyi S, Lee KD, Rogers SE, Kwak D. High-lift design optimization using Navier–Stokes equations. J Aircr 1996;33(3):499–504.
[53] Fejtek I. Summary of code validation results for a multiple element airfoil test case. AIAA Paper 97-1932, June–July 1997.
[54] Fiddes SP, Kirby DA, Woodward DS, Peckham DH. Investigation into the effects of scale and compressibility on lift and drag in the RAE 5 m pressurized low-speed wind tunnel. AGARD CP-365, 1984, May, paper 2. Also RAE-TM-AERO-2006, June 1984.
[55] Foster DN, Irwin HPAH, Williams BR. The two-dimensional flow around a slotted flap. RAE R&M 3681, September 1970.
[56] Fritz W. Calculation of maximum and high lift characteristics of multi element airfoils. AGARD CP-515, September, 1993. p. 5.1–5.12.
[57] Garner PL, Meredith PT, Stoner RC. Areas for future CFD development as illustrated by transport aircraft applications. AIAA Paper 91-1527, June 1991.
[58] Gatlin GM, McGhee RJ. Experimental investigation of semispan model testing techniques. J Aircr 1997;34(4):500–5.
[59] Godin P, Zingg DW, Nelson TE. High-lift aerodynamic computations with one- and two-equation turbulence models. AIAA J 1997;35(2):237–43; Also AIAA Paper 96-0567, January 1996.
[60] Gooden JHM, van Lent M. Hot-wire measurements in the two-dimensional wing wake above a trailing edge flap at a condition close to maximum lift. NLR CR 91038 C (restricted), The Netherlands, 1991.
[61] Greenman RM, Roth KR. Minimizing computational data requirements for multi-element airfoils using neural networks. J Aircr 1999;36(5):777–84.
[62] Haines AB. Scale effects on aircraft and weapon aerodynamics. AGARDograph 323, July 1994.
[63] Haines AB. Scale effect on $C_{L,\max}$ at high Reynolds number. High lift and separation control, Proceedings of the Conference, University of Bath, UK, March 1995. London: Royal Aeronautical Society, 1995. p. 28.1–28.14.
[64] Hobbs CR, Spaid F, Ely W, Goodman W. High lift research program for a fighter-type multi-element airfoil at high Reynolds numbers. AIAA Paper 96-0410, January 1996.
[65] Hung K, Papadakis M, Wong S-H, Wong S-C. Computation of pre- and post-stall flows over single and multi-element airfoils. AIAA Paper 98-0756, January 1998.
[66] Hussaini MY, Morrison JH, Woodruff SL. Evaluation of several turbulence models in a multiple-element airfoil computation. AIAA Paper 98-0327, January 1998.
[67] Hyams DG, Sreenivas K, Sheng C, Briley WR, Marcum DL, Whitfield DL. An investigation of parallel implicit solution algorithms for incompressible flows on multi-element unstructured topologies. AIAA Paper 2000-0271, January 2000.
[68] Jacob K. A fast computing method for the flow over high-lift wings. AGARD CP-515, September, 1993. p. 23.1–23.12.

[69] Jahangirian AR, Johnston LJ. Calculation of high-lift aerodynamics on adaptive unstructured grids. International Council of the Aeronautical Sciences Proceedings, 20th Congress, vol. 2. Reston, VA: AIAA, 1996. p. 2221–31.
[70] Jasper DW, Agrawal S, Robinson BA. Navier–Stokes calculations on multi-element airfoils using a chimera-based solver. AGARD CP-515, September, 1993. p. 8.1–8.11.
[71] Johnson PL, Jones KM, Madson MD. Experimental investigation of a simplified 3d high lift configuration in support of CFD validation. AIAA Paper 2000-4217, August 2000.
[72] Johnston LJ, Stolcis L. Prediction of the high-lift performance of multi-element aerofoils using an unstructured Navier-Stokes solver. AGARD CP-515, September, 1993. p. 13.1–13.18.
[73] Jones KM, Biedron RT, Whitlock M. Application of a Navier–Stokes solver to the analysis of multielement airfoils and wings using multizonal grid techniques. AIAA Paper 95-1855, June 1995.
[74] Kalitzin G. Application of turbulence models to high-lift airfoils. Center for Turbulence Research, Annual Research Briefs, December 1997. p. 165–77.
[75] Kern S. Evaluation of turbulence models for high-lift military airfoil flowfields. AIAA Paper 96-0057, January 1996.
[76] Khorrami MR, Singer BA, Radeztsky Jr. RH. Reynolds averaged Navier–Stokes computations of a flap side-edge flow field. AIAA J 1999;37(1):14–22.
[77] Kim CS, Kim C, Rho OH. Parallel computations of high-lift airfoil flows using two-equation turbulence models. AIAA J 2000;38(8):1360–8; Also AIAA Paper 99-0542, January 1999.
[78] Kim CS, Kim C, Rho OH. Sensitivity analysis for the Navier–Stokes equations with two-equation turbulence models. AIAA J 2001;39(5):838–45.
[79] Kim S, Alonso JJ, Jameson A. Two-dimensional high-lift aerodynamic optimization using the continuous adjoint method. AIAA Paper 2000-4741, September 2000.
[80] King DA, Williams BR. Developments in computational methods for high-lift aerodynamics. Aeronaut J 1988;92(917):265–88.
[81] Klausmeyer SM, Lin JC. An experimental investigation of skin friction on a multi-element airfoil. AIAA Paper 94-1870, June 1994.
[82] Klausmeyer SM, Lin JC. Comparative results from a CFD challenge over a 2d three-element high-lift airfoil. NASA TM 112858, May 1997.
[83] Kogan A, Marom S. Navier-Stokes calculations of the flow about wing-flap combinations. International Council of the Aeronautical Sciences Proceedings, 18th Congress, vol. 1. Reston, VA: AIAA, 1992. p. 108–21.
[84] Kusunose K, Cao HV. Prediction of transition location for a 2-d Navier–Stokes solver for multi-element airfoil configurations. AIAA Paper 94-2376, June 1994.
[85] Kusunose K, Cao HV. Numerical prediction of reverse Reynolds number effects for multi-element airfoils. In: Taylor C, Durbetaki P, editor. Numerical methods in laminar and turbulent flow, vol. 9, part 1. Swansea, UK: Pineridge Press, 1995. p. 457–68.
[86] Kusunose K, Wigton L, Meredith P. A rapidly converging viscous/inviscid coupling code for multi-element airfoil configurations. AIAA Paper 91-0177, January 1991.
[87] Laia JR. Analysis, test report of 2-d wind tunnel test of a 13% super-critical airfoil section fitted with various blown and mechanical flap high lift systems. Grumman Aerospace Corporation Report XA128-900-2, July 1983.
[88] Larsson T. Separated and high-lift flows over single and multi-element airfoils. International Council of the Aeronautical Sciences Proceedings, 19th Congress, vol. 3. Reston, VA: AIAA, 1994. p. 2505–18.
[89] LeBalleur JC, Neron M. A viscous-inviscid solver for high-lift incompressible flows over multi-element airfoils at deep separation conditions. AGARD CP-515, September, 1993. p. 11.1–11.12.
[90] Lien FS, Chen WL, Leschziner MA. Computational modelling of high-lift aerofoils with turbulence-transport models. High lift and separation control, Proceedings of the Conference, University of Bath, UK, March 1995. London: Royal Aeronautical Society, 1995. p. 10.1–10.14.
[91] Lin JC, Dominik CJ. Parametric investigation of a high-lift airfoil at high Reynolds numbers. J Aircr 1997;34(4):485–91.
[92] Lindblad IAA, de Cock KMJ. CFD prediction of maximum lift of a 2d high lift configuration. AIAA Paper 99-3180, June–July 1999.
[93] Liou WW, Liu F. Computational modeling for the flow over a multi-element airfoil. AIAA Paper 99-3177, June–July 1999.
[94] Liou WW, Liu F. Computational modeling for the transitional flow over a multi-element airfoil. AIAA Paper 2000-4322, August 2000.
[95] Lorentzen L, Lindblad IAA. Application of two-equation and EARSM turbulence models to high lift aerodynamics. AIAA Paper 99-3181, June–July 1999.
[96] Lovell DA. A wind-tunnel investigation of the effects of flap span and deflection angle, wing planform and a body on the high-lift performance of a 28° swept wing. RAE CP No. 1372, Farnborough, UK, 1977.
[97] Lyapunov SV, Wolkov AV. Application of viscous-inviscid interaction methods for a separated flow calculation about airfoils and high-lift systems. International Council of the Aeronautical Sciences Proceedings, 20th Congress, vol. 2. Reston, VA: AIAA, 1996. p. 2194–202.
[98] Lynch FT, Potter RC, Spaid FW. Requirements for effective high lift CFD. International Council of the Aeronautical Sciences Proceedings, 20th Congress, vol. 2. Reston, VA: AIAA, 1996. p. 1479–92.
[99] Mathias DL, Roth KR, Ross JC, Rogers SE, Cummings RM. Navier–Stokes analysis of the flow about a flap edge. AIAA Paper 95-0185, January 1995.
[100] Mavriplis DJ. Three-dimensional high-lift analysis using a parallel unstructured multigrid solver. AIAA Paper 98-2619, June 1998.
[101] Mavriplis DJ, Pirzadeh S. Large-scale parallel unstructured mesh computations for three-dimensional high-lift analysis. J Aircr 1999;36(6):987–98; Also AIAA Paper 99-0537, January 1999.
[102] McGinley CB, Anders JB, Spaid FW. Measurements of Reynolds stress profiles on a high-lift airfoil. AIAA Paper 98-2620, June 1998.

[103] Menter FR. Two-equation eddy-viscosity turbulence models for engineering applications. AIAA J 1994;32(8): 1598–605.
[104] Menter FR. Eddy viscosity transport equations, their relation to the k–ε model. J Fluids Eng 1997;119(12):876–84.
[105] Meredith PT. Viscous phenomena affecting high-lift systems and suggestions for future CFD development. AGARD CP-515, September, 1993. p. 19.1–19.8.
[106] Moir IRM. Measurements on a two-dimensional aerofoil with high-lift devices. AGARD AR-303, August, 1994. p. A2.1–A2.12.
[107] Moitra A. Validation of an automated CFD tool for 2-d high-lift analysis. AIAA Paper 2001–2401, June 2001.
[108] Morrison JH. Numerical study of turbulence model predictions for the MD 30P/30N and NHLP-2D three-element highlift configurations. NASA/CR-1988-208967, December 1998.
[109] Nakayama A, Kreplin HP, Morgan HL. Experimental investigation of flowfield about a multielement airfoil. AIAA J 1990;28(1):14–21.
[110] Nash SM, Rogers SE. Numerical study of a trapezoidal wing high-lift configuration. SAE Paper 1999-01-5559, October 1999.
[111] Nelson TE, Godin P, De Rango S, Zingg DW. Flow computations for a three-element airfoil system. Can Aeronaut Space J 1999;45(2):132–9; Also Sixth CASI Aerodynamics Symposium Proceedings, Canadian Aeronautics and Space Institute, Ottawa, 1997. p. 357–66.
[112] Nelson TE, Godin P, Zingg DW. Multi-element airfoil computations with one-equation turbulence models. AIAA Paper 95-0357, January 1995.
[113] Nelson TE, Zingg DW, Johnston GW. Compressible Navier-Stokes computations of multielement airfoil flows using multiblock grids. AIAA J 1994;32(3):506–11.
[114] Nield BN. An overview of the 777 high lift aerodynamic design. Aeronaut J 1995;99(989):361–71; Also High lift and separation control, Proceedings of the Conference, University of Bath, UK. London: Royal Aeronautical Society, March 1995. p. 1.1–1.14.
[115] Oliver WR. Results of design studies and wind tunnel tests of an advanced high-lift system for an energy efficient transport. NASA CR-159389, December 1980.
[116] Olson LE, Orloff KL. On the structure of turbulent wakes and merging shear layers of multi-element airfoils. AIAA Paper 81-1238, June 1981.
[117] Omar E, Zierten T, Mahal A. Two-Dimensional wind tunnel tests of a NASA supercritical airfoil with various high lift systems, vol. I—data analysis. NASA CR-2214, April 1977.
[118] Omar E, Zierten T, Hahn M, Szpiro E, Mahal A. Two-Dimensional wind tunnel tests of a NASA supercritical airfoil with various high lift systems, vol. II—test data. NASA CR-2215, April 1977.
[119] Omer ME. Wind tunnel investigation of single, double, and triple-slotted trailing-edge flaps. Boeing Document D6-41068TN, 1973.
[120] Paschal K, Jenkins L, Yao C. Unsteady slat-wake characteristics of a high-lift configuration. AIAA Paper 2000-0139, January 2000.
[121] Payne FM. LTPT 2d wind tunnel test of a single slotted flap and comparison with a 2d Navier–Stokes code. Boeing Document D6-81693, 1995.
[122] Payne FM, Wyatt GW, Bogue DR, Stoner RC. High Reynolds number studies of a Boeing 777-200 high lift configuration in the NASA ARC 12′ pressure tunnel and NASA LaRC national transonic facility. AIAA Paper 2000-4220, August 2000.
[123] Petrov AV. Certain types of separated flow over slotted wings. Fluid Mech—Sov Res 1978;7(5):80–9.
[124] Petrov AV. Separated flow about high-lift wings and active control. High lift and separation control, Proceedings of the Conference, University of Bath, UK. London: Royal Aeronautical Society, March 1995. p. 20.1–20.7.
[125] Porcheron B, Thibert JJ. Etude detailee de l-ecolement autour d'un profil hypersustente, comparisons avec les calculs. AGARD Symposium on Improvement of Aerodynamic Performance Through Boundary Layer Control and High-Lift Systems, Brussels, May 1984.
[126] Potter RC, van Dam CP, Hardin JD. Viscous-flow analysis of a subsonic transport high-lift system including comparisons with flight-measured results. AIAA Paper 95-0043, January 1995.
[127] Puffert-Meibner W. ALVAST half-model wind tunnel investigations and comparison with full-span model results. DLR IB 129-96/20, 1996.
[128] Radeztsky Jr RH, Singer BA, Khorrami MR. Detailed measurements of a flap side-edge flow field. AIAA Paper 98-0700, January 1998.
[129] Ravachol M. Unstructured finite element for incompressible flows. AIAA Paper 97-1864, June–July 1997.
[130] Rogers SE. Progress in high-lift aerodynamic calculations. J Aircr 1994;31(6):1244–51; Also AIAA Paper 93-0194, January 1993.
[131] Rogers SE, Cao HV, Su TY. Grid generation for complex high-lift configurations. AIAA Paper 98-3011, June 1998.
[132] Rogers SE, Menter FR, Durbin PA, Mansour NN. A comparison of turbulence models in computing multi-element airfoil flows. AIAA Paper 94-0291, January 1994.
[133] Rogers SE, Roth K, Cao HV, Slotnick JP, Whitlock M, Nash SM, Baker MD. Computation of viscous flow for a Boeing 777 aircraft in landing configuration. J Aircr 2001;38(6):1060–8; Also AIAA Paper 2000-4221, August 2000.
[134] Rogers SE, Roth K, Nash SM. Validation of computed high-lift flows with significant wind-tunnel effects. AIAA J 2001;39(10):1884–92; Also AIAA Paper 2000-4218, August 2000.
[135] Rogers SE, Roth K, Nash SM, Baker MD, Slotnick JP, Whitlock M, Cao HV. Advances in overset CFD processes applied to subsonic high-lift aircraft. AIAA Paper 2000-4216, August 2000.
[136] Rogers SE, Wiltberger NL, Kwak D. Efficient simulation of incompressible viscous flow over multi-element airfoils. AGARD CP-515, September, 1993. p. 7.1–7.9; Also Proceedings of the Fifth Symposium on Numerical and Physical Aspects of Aerodynamic Flows, California State University, Long Beach, CA, January 1992; Also NASA CR-193000, Part 1, January 1992.
[137] Rudnik R, Melber S, Ronzheimer A, Brodersen O. Three-dimensional Navier-Stokes simulations for transport

aircraft high-lift configurations. J Aircraft 2001;38(5): 895–903; Also AIAA Paper 2000-4326, August 2000.
[138] Rumsey CL, Gatski TB. Recent turbulence model advances applied to multielement airfoil computations. J Aircraft 2001;38(5):904–10; Also AIAA Paper 2000-4323, August 2000.
[139] Rumsey CL, Gatski TB, Ying SX, Bertelrud A. Prediction of high-lift flows using turbulent closure models. AIAA J 1998;36(5):765–74; Also AIAA Paper 97-2260, June 1997.
[140] Rumsey CL, Lee-Rausch EM, Watson RD. Three-dimensional effects on multi-element high-lift computations. AIAA Paper 2002-0845, January 2002.
[141] Schonfeld T, Corjon A, Rudnik R, Ronzheimer A, Elphick G, Galpin S. Wake vortex analysis of a high-lift aircraft configuration on structured and unstructured grids. AIAA Paper 2000-2218, June 2000.
[142] Schuster DM, Birckelbaw LD. Numerical computation of viscous flowfields about multiple component airfoils. AIAA Paper 85-0167, January 1985.
[143] Shima E, Egami E, Amano K. Navier–Stokes computation of a high lift system using Spalart-Allmaras turbulence model. AIAA Paper 94-0162, January 1994.
[144] Slotnick JP, An MY, Mysko SJ, Yeh DT. Navier-Stokes analysis of a high wing transport high-lift configuration with externally blown flaps. AIAA Paper 2000-4219, August 2000.
[145] Smith AMO. High-lift aerodynamics. J Aircr 1975;12(6):501–30.
[146] Smith AMO. Wing design, analysis—your job. Proceedings of the Second Symposium on Numerical and Physical Aspects of Aerodynamic Flows, California State University, Long Beach, CA, January 1983: keynote lecture 1.
[147] Spaid FW. High Reynolds number, multielement airfoil flowfield measurements. J Aircr 2000;37(3):499–507; Also AIAA Paper 96-0682 (Spaid FW, Lynch FT), January 1996.
[148] Spalart PR, Allmaras SR. A one-equation turbulence model for aerodynamic flows. La Recherche Aerospatiale 1994;1:5–21.
[149] Squire LC. Interactions between wakes and boundary-layers. Prog Aerospace Sci 1989;26:261–88.
[150] Stenewsky E, Thibert JJ. Airfoil SKF 1.1 with maneuver flap. AGARD AR-138, May, 1979. p. A5.1–A5.29.
[151] Stolcis L. Computation of the turbulent flow over a high-lift system using an algebraic Reynolds stress model. In: Taylor C, editor. Numerical methods in laminar and turbulent flow, vol. 8, part 2. Swansea, UK: Pineridge Press, 1993. p. 1009–20.
[152] Stolcis L. Navier-Stokes solution of compressible fluid flows using advanced turbulence models and unstructured grids. In: Morton KW, Baines MJ, editors. Numerical methods for fluid dynamics V. Oxford, UK: Clarendon Press, 1995. p. 591–7.
[153] Stolcis L, Johnston LJ. Application of an unstructured Navier–Stokes solver to multi-element airfoils operating at transonic maneuver conditions. AIAA Paper 92-2638-CP, June 1992.
[154] Storms BL, Ross JC, Horne WC, Hayes JA, Dougherty RP, Underbrink JR, Scharpf DF, Moriarty PJ. An aeroacoustic study of an unswept wing with a three-dimensional high-lift system. NASA TM-112222, February 1998.
[155] Storms BL, Takahashi TT, Ross JC. Aerodynamic influence of a finite-span flap on a simple wing. SAE Paper 95-1977, SAE Aerotech 95, Los Angeles, CA, September 1995.
[156] Szmelter J, Cross MR. Applications of unstructured meshes techniques to high lift configurations. High lift and separation control, Proceedings of the Conference, University of Bath, UK. London: Royal Aeronautical Society, March 1995. p. 9.1–9.13.
[157] Szodruch J, Kotschote J. Grenzschichtmessungen an einem transsonikprofil in MBB-LSWT. Ergebnisbericht Nr. 36, MBB GmbH., 1983.
[158] Takallu MA. Reynolds-averaged Navier-Stokes computations of a high-lift transport model with and without semi-span standoff. AIAA Paper 2000-4222, August 2000.
[159] Takallu MA, Laflin KR. Reynolds-averaged Navier-Stokes simulations of two partial-span flap wing experiments. AIAA Paper 98-0701, January 1998.
[160] Taki M, Johnston LJ. Application of a block-structured Navier-Stokes solver for high-lift aerofoil applications. Proceedings of the Seventh Biennial Colloquium on Computational Fluid Dynamics, University of Manchester Institute of Science and Technology, UK, May 1996. p. 3.5–3.6.
[161] Thibert JJ. The GARTEUR high lift research programme. AGARD CP-515, September, 1993. p. 16.1–16.21.
[162] Thibert JJ, Reneaux J, Moens F, Priest J. ONERA activities on high-lift devices for transport aircraft. Aeronaut J 1995;99(989):395–411; Also High lift and separation control, Proceedings of the Conference, University of Bath, UK. London: Royal Aeronautical Society, March 1995. p. 5.1–5.18.
[163] Thomas JL, Salas MD. Far-field boundary conditions for transonic lifting solutions to the Euler equations. AIAA J 1986;24(7):1074–80.
[164] Valarezo WO. High lift testing at high Reynolds numbers. AIAA Paper 92-3986, July 1992.
[165] Valarezo WO. Topics in high-lift aerodynamics. AIAA Paper 93-3136, July 1993.
[166] Valarezo WO, Chin VD. Method for the prediction of wing maximum lift. J Aircr 1994;31(1):103–9; Also Maximum lift prediction for multielement wings. AIAA Paper 92-0401, January 1992.
[167] Valarezo WO, Dominik CJ, McGhee RJ. Reynolds and Mach number effects on multielement airfoils. Proceedings of the Fifth Symposium on Numerical and Physical Aspects of Aerodynamic Flows, California State University, Long Beach, CA, January 1992; Also NASA CR-193000, Part 1, January 1992.
[168] Valarezo WO, Dominik CJ, McGhee RJ, Goodman WL, Paschal KB. Multi-element airfoil optimization for maximum lift at high Reynolds numbers. AIAA Paper 91-3332-CP, September 1991.
[169] Valarezo WO, Mavriplis DJ. Navier–Stokes applications to high-lift airfoil analysis. J Aircr 1995;32(3):618–24; Also AIAA Paper 93-3534, August 1993.

[170] Van den Berg B. Boundary layer measurements on a two-dimensional wing with flap. National Aerospace Laboratory Data Report NLR TR 79007 U, The Netherlands, 1979.

[171] Van den Berg B, Oskam B. Boundary-layer measurements on a two-dimensional wing with flap and a comparison with calculations. AGARD CP-271, 1979. p. 18.1–18.14.

[172] Van Lent M, Buning LR, Rohne PB. High lift experiments on the GARTEUR AD (AG08) two-dimensional model M3 in the NLR LST and HST wind tunnels. National Aerospace Laboratory Data Report NLR TR 89124 C, The Netherlands, 1989.

[173] Verhoff A, Michal T, Cebeci T. An accurate and efficient viscous interaction approach for analysis and design of airfoils and high-lift configurations. International Council of the Aeronautical Sciences Proceedings, 20th Congress, vol. 2. Reston, VA: AIAA, 1996. p. 2203–13.

[174] Wentz WH, Seetharam HC. Development of a Fowler flap system for a high performance general aviation airfoil. NASA CR-2443, December 1974.

[175] Wentz WH, Seetharam HC, Fiscko KA. Force and pressure tests of the GA(W)-1 airfoil with a 30% Fowler flap. NASA CR-2833, June 1977.

[176] Weston R. Refinement of a method for determining the induced and profile drag of a finite wing from detailed wake measurements. Ph.D. dissertation, University of Florida, 1981.

[177] Whitcomb RT, Clark LR. An airfoil shape for efficient flight at supercritical Mach numbers. NASA TM-X-1109, 1965.

[178] Wilcox DW. Turbulence modeling for CFD. 2nd ed. La Canada: DCW Industries, 1998.

[179] Wild JW. Direct optimization of multi-element-airfoils for high-lift using Navier–Stokes equations. Computational fluid dynamics 98. Proceedings of the Fourth European Computational Fluid Dynamics Conference, Athens Greece, Part 1, September 1998. p. 383–90.

[180] Williams B. An exact test case for the plane potential flow about two adjacent lifting airfoils. RAE Report 3717, 1971.

[181] Wilquem F, Passelecq C, Degrez G. A block structured based method for the flow prediction over low Reynolds number multi-element airfoils. International Council of the Aeronautical Sciences Proceedings, 20th Congress, vol. 2. Reston, VA: AIAA, 1996. p. 2232–41.

[182] Woodward DS, Hardy BC, Ashill PR. Some types of scale effect in low-speed, high-lift flows. International Council of the Aeronautical Sciences Proceedings, 16th Congress, vol. 2. Reston, VA: AIAA, 1988. p. 1402–16.

[183] Woodward DS, Lean DE. Where is high lift today?—a review of past UK research programmes. AGARD CP-515, September, 1993. p. 1.1–1.45.

[184] Ying SX. High lift: challenges and directions for CFD. Proceedings of the Northwestern Polytechnical University/AIAA Atmospheric Flight Mechanics Conference, Northwestern Polytechnical University, Xian, PRC, 1996. p. 164–77.

[185] Ying SX, Spaid FW, McGinley CB, Rumsey CL. Investigation of confluent boundary layers in high-lift flows. J Aircr 1999;36(3):550–62; Also AIAA Paper 98-2622, June 1998.

[186] Yip LP, van Dam CP, Whitehead JH, Hardin JD, Miley SJ, Potter RC, Bertelrud A, Edge DC, Willard PE. The NASA B737-100 high-lift flight research programme—measurements and computations. Aeronaut J 1995;99 (989):372–86; Also High lift and separation control, Proceedings of the Conference, University of Bath, UK. London: Royal Aeronautical Society, March 1995. p. 27.1–27.20.

[187] Yip LP, Vijgen PMHW, Hardin JD, Van Dam CP. In-flight pressure distributions and skin-friction measurements on a subsonic transport high-lift wing section. AGARD CP-515, September, 1993. p. 21.1–21.19.